Journal of Medicinal Chemistry

Article

Imidazo[1,2-a]pyridine Derivatives as Aldehyde Dehydrogenase Inhibitors: Novel Chemotypes to Target Glioblastoma Stem Cells.

Luca Quattrini, Edoardo Luigi Maria Gelardi, Vito Coviello, Stefania Sartini, Davide Ferraris, Mattia Mori, Ichiro Nakano, Silvia Garavaglia, and Concettina La Motta

J. Med. Chem., **Just Accepted Manuscript** • DOI: 10.1021/acs.jmedchem.9b01910 • Publication Date (Web): 30 Mar 2020

Imidazo[1,2-*a*]pyridine Derivatives as Aldehyde Dehydrogenase Inhibitors: Novel Chemotypes to Target Glioblastoma Stem Cells.

Luca Quattrini,[§ç] Edoardo Luigi Maria Gelardi,[£ç] Vito Coviello,[§] Stefania Sartini,[§] Davide Maria Ferraris,[£] Mattia Mori,[#] Ichiro Nakano,[$] Silvia Garavaglia,[£*] Concettina la Motta.[§*]

[§]*Department of Pharmacy, University of Pisa, Via Bonanno 6, 56126, Pisa, Italy.*

[£]*Department of Drug Science, University of Piemonte Orientale, Via Bovio 6, 28100, Novara, Italy.*

[#]*Department of Biotechnology, Chemistry and Pharmacy "Department of Excellence 2018-2022", University of Siena, via Aldo Moro 2, Siena, Italy.*

[$]*Department of Neurosurgery, University of Alabama at Birmingham, WTI 401, 1824 6th Avenue South, Birmingham, Alabama 35233.*

Abstract

Glioblastoma multiforme (GBM) is the deadliest form of brain tumour. It is known for its ability to escape the therapeutic options available to date, thanks to the presence of a subset of cells endowed with stem-like properties and able to resist to cytotoxic treatments. As the cytosolic enzyme aldehyde dehydrogenase 1A3 turns out to be overexpresses in this kind of cells, playing a key role for their vitality, treatments targeting this enzyme may represent a successful strategy to fight GBM. In this work we describe a novel class of imidazo[1,2-*a*]pyridine derivatives as aldehyde dehydrogenase 1A3 inhibitors, reporting the evidence of their significance as novel drug candidates for the treatment of GBM. Besides showing an interesting functional profile, in terms of activity against the target enzyme and selectivity toward highly homologous isoenzymes, representative examples of the series showed also a nanomolar to picomolar efficacy against patient-derived GBM stem-like cells, thus proving the concept that targeting aldehyde dehydrogenase might represent a novel and promising way to combat GBM by striking its ability to divide immortally.

Introduction

Glioblastoma multiforme (GBM) is the most aggressive and fast-growing astrocytic tumour, accounting for about 15% of all brain tumours in adults. Although rare at presentation, with a yearly incidence of about two to three per 100.000 adults in both North America and Europe, GBM represents a critical health issue due to its unavoidably poor prognosis.[1]

The treatment of choice for GMB relies in the maximal surgical resection of the tumour mass, associated with external beam radiation therapy and the adjuvant administration of temozolomide (Chart 1). However, the remarkable toxicity of the therapeutic intervention, combined with both its marginal efficacy and the emergence of relapse, generally limit the median survival of the treated patients to approximately 14 to 15 months from the diagnosis, with less than 5% surviving over 5 years.[2] Accordingly, a ground-breaking therapeutic solution for people affected by GBM is urgently needed.

Chart 1. Temozolomide and Aldehyde Dehydrogenase Inhibitors under Investigation

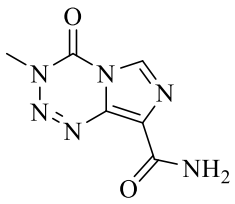

Temozolomide

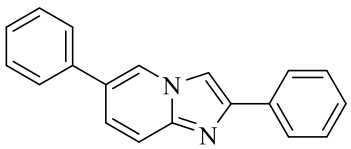

GA11

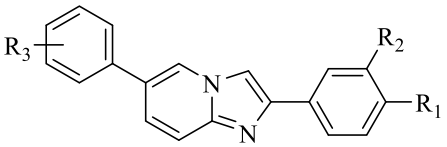

3a-v

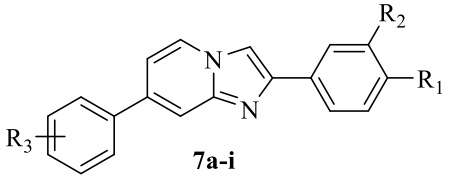

7a-i

As a malignancy, GBM is made of a heterogeneous community of different cells governed by cooperative interactions.[3,4] A small percentage of them, bearing stem-like properties, plays more

than most a key role in tumour perpetuating and progression, being endowed with indefinite self-renewal ability and aberrant differentiation capacity.[5,6]

Differently from tumour bulk cells, glioma stem-like cells (GSCs) are able to resist to cytotoxic treatments commonly exploited to target rapidly dividing cells, as they are characterized by a slow mitotic activity possibly associated with a quiescent G0/G1 state. Hence, rather than being eradicated, GSCs turn out to be selected over the cancer bulk, being free to drive tumour relapse and mediate metastasis. Therefore, they represent the reference sub-population that should be brought into focus, as undermining self-renewal signaling pathways supporting their growth and residence in the stem state may represent an effective strategy to wipe out efficiently the whole tumour architecture. Indeed, experience gained in the management of different malignancies proof the concept that targeting cancer stem cells improve patient outcomes by preventing tumours recurrences,[7] increasing chemotherapy efficacy[8] and reversing chemotherapy resistance.[9]

To date, two distinct and mutually exclusive population of GSCs have been differentiated by transcriptome array analyses, namely the proneural (PN-) and the mesenchymal (MES-) one, strictly correlated to the clinically relevant proneural and mesenchymal subtypes of GBM.[10]

While the PN-GSC subtype tends to adopt a MES identity in response to radiation treatment, MES-GSCs display a well-characterized profile, turning out to be an aggressive phenotype markedly resistant to radiation and showing high expression of genes associated with DNA repair. MES-GSCs exhibit also high levels of the cytoplasmic enzyme aldehyde dehydrogenase, subtype 1A3 (ALDH1A3). Besides being acknowledged as the distinctive hallmark of this type of cancer cell sub-population, ALDH1A3 plays also a crucial role in stem cells vitality, being involved in the differentiation of progenitor cells into mature entities. Its overexpression endorses high grade gliomas and is decisive for tumor invasion, thus having a prognostic value for poor clinical outcomes.[10,11] Accordingly, targeting this enzyme might represent a successful strategy to put in place a keystone molecular treatment of GBM.

By exploiting a rational approach, we recently succeeded in turning the natural ALDH inhibitor daidzin into a novel effective derivative, 2,6-diphenylimidazo[1,2-*a*]pyridine, namely GA11 (Chart 1, compound **3a** in Table 2), which proved to combine a significant *in vitro* inhibitory activity against the target enzyme with a potent *in vivo* anti-tumor efficacy when administered in a murine GSC-derived xenograft model of GBM.[12] Taken together, these results were extremely encouraging as they affirmed GA11 as a sound and viable candidate deserving of further development.

Therefore, guided by a preliminary crystallization study, performed to highlight GA11 accommodation into the active site of ALDH1A3, we embarked in the structural optimization of the hit compound with the purpose to obtain a novel and effective class of ALDH1A3 inhibitors.

In this work, we present the synthesis of novel derivatives of GA11, whose phenyl rings in both positions 2 and 6 of the heterocyclic core were suitably modified in their electronic and steric features through the insertion suitable substituents. All the synthesized compounds were evaluated in vitro for their activity against the target ALDH1A3 and selectivity towards the parent ALDH1A1 and ALDH1A2 subtypes, as well as for their anti-proliferative activity toward selected GBM cell lines. Results obtained were rationalised through molecular docking reasoning.

Results and Discussion

Crystallization study. The development of a compound able to target the human ALDH1A3 is a difficult challenge, especially when a selectivity profile for the 1A1 and 1A2 isoenzymes is also pursued. Therefore, an integrated approach that would use both structural studies and in silico drug design is advisable. All the ALDH1A isoenzymes are able to catalyze the conversion of the natural substrate retinal to retinoic acid, but they show preferences for a different isomer of retinal. ALDH1A3, in particular, has a major affinity for all-trans retinal. It implies some diversity in the features defining the catalytic site of the different isoforms, which should be taken into consideration to get to novel active and selective derivatives.[13] Indeed, the geometry of the substrate access tunnel has a central role in ALDHs specificity.

We started our research project co-crystallizing the reference hit GA11 (**3a** from here on out), with the human recombinant ALDH1A3, to begin deciphering its binding mode to the target enzyme (Figure 1, PDB code:6S6W). The obtained three-dimensional structure of human ALDH1A3 in complex with **3a** has been solved by molecular replacement using the human ALDH1A3 atomic coordinates as a search model (PDB code: 5FHZ[14]), and refined at a resolution of 3.2 Å (Figure 1). The final human ALDH1A3 model contains two identical chains per asymmetric unit, arranged as dimer, and a total of 11 solvent molecules (Table 1).

Table 1. Data collection and refinement statistics of the three-dimensional structure of human ALDH1A3 in complex with compounds **3a** (PDB code: 6S6W) and **3q** (PDB code: 6TE5).

Data Collection		
	Compound 3a[a]	**Compound 3b**[b]
Space group	$P2_122_1$	$P2_122_1$
Cell dimensions		
a, b, c (Å)	81.6 89.4 159.0	81.2 89.4 159.2
a, b, c (°)	90, 90, 90	90, 90, 90
Resolution (Å)	48.02 - 3.2	48.02 - 3.2
R_{pim}/R_{merge}	0.064 (0.399)/0.128 (0.787)	0.076 (0.399)/0.168 (0.772)
Mean(I) / sd(I)	9.8 (2.1)	8.9 (2.4)
Completeness (%)	99.4 (99.3)	99.8 (99.3)
Redudancy	4.7 (4.6)	5.6 (5.9)
Refinement		
Resolution (Å)	3.2	3.2
No. reflections	18833 (1840)	18833 (1823)
R_{work} /R_{free}	0.19 / 0.26	0.18 / 0.24
No. atoms		
Protein	7446	7446
Water	11	20
Ligands	121	148
Mean B-factors		
Protein ($Å^2$)	77.6	56.7

Water (Å^2)	52.4	48.3
Ligands (Å^2)	94.8	82.9
R.m.s. deviations		
Bond lengths (Å)	0.006	0.014
Bond angles (°)	1.10	1.63
Ramachandran outliers (%)	0.5	0.2

[a]PDB deposition name: GA11. [b]PDB deposition name: LQ43.

The structure analysis confirms that the obtained **3a**-ALDH1A3 complex folds into 13 α-helices, 19 β-strands and the connecting loops, arranged into three functional domains. Both the NAD^+ binding domain and the catalytic domain are built on a topologically related βαβ type polypeptide fold (Figure 1A). Our crystallographic data revealed that, in all monomers, **3a** binds to the enzyme at the entrance of the tunnel, which therefore turns out to be partially clogged by the compound. It is important to highlight that **3a** is a symmetric compound, and its phenyl rings at position 2 and 6 of the imidazo[1,2-*a*]pyridine scaffold can binds the enzyme site in two overturned, almost equivalent conformations Therefore, to fully unveil the binding mode of the compound, we decided to make use of docking simulations. Molecular modelling was carried out by GOLD docking program[15] towards the crystallographic structure of ALDH1A3 described above, and solved in complex with **3a**. Results clearly show that two possible binding modes of **3a** are possible, depicted in Figure 2. They both share a comparable affinity, with a slightly higher theoretical affinity for the binding mode described in Figure 2A, where the phenyl ring in position 6 of the imidazo[1,2-*a*]pyridine scaffold is projected toward the binding site flanked by residues G136, L185, T189, L471, and A473. It is worth noting that this is the same site occupied by the cyclohexene ring of the natural ligand retinoic acid, such as recently highlighted by X-ray crystallography.[14] By adopting this pose, **3a** casts the 2-phenyl ring toward the side chain of the aromatic F308, thus allowing a π-π stacking interaction which makes the compound binding more effective. No poses were found within the hydrophobic pocket of the catalytic site, in proximity to the catalytic residues.

Figure 1. Overall monomer structure of human ALDH1A3 in complex with **3a** (PDB code: 6S6W, PDB deposition name GA11).

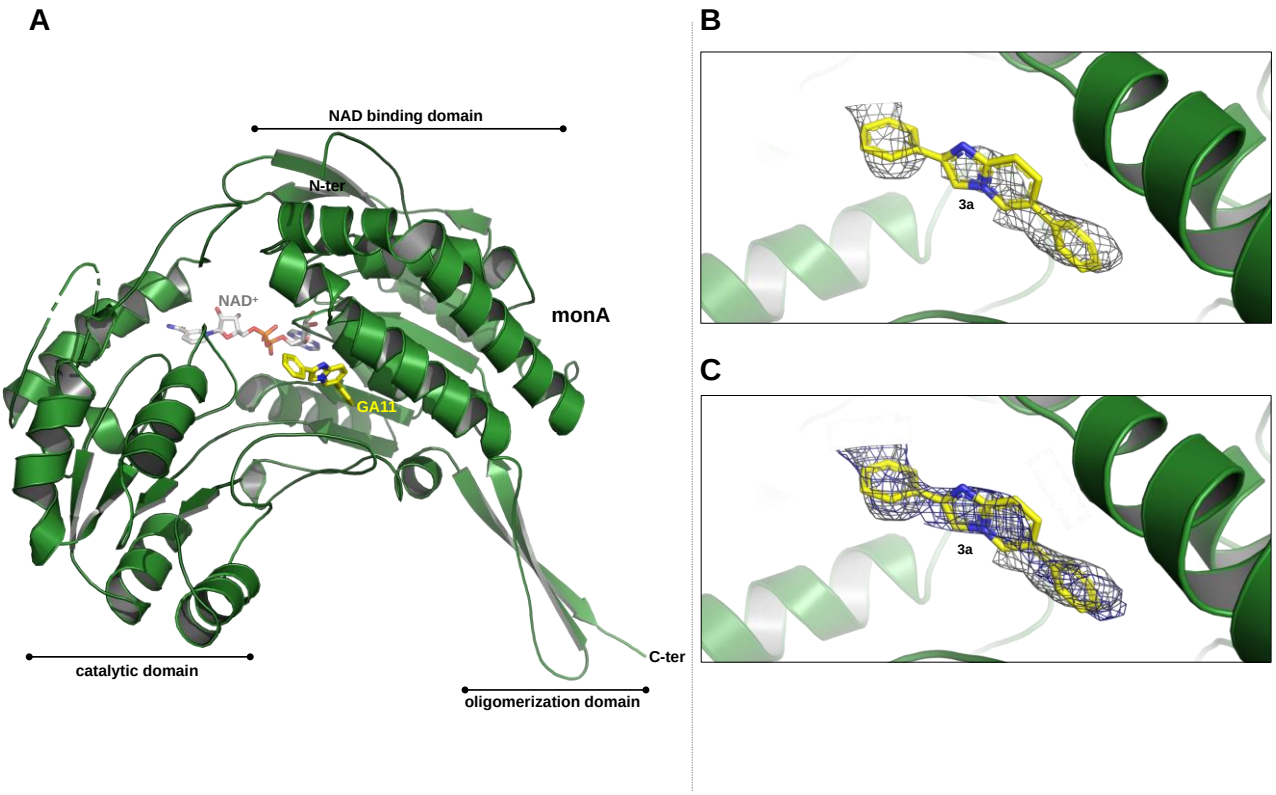

Panel A. Ribbon representation of the overall structure of the monomer of ALDH1A3. Each monomer consists of three domains: the NAD^+ binding-domain, the catalytic-domain and the oligomerization domain. The ligands **3a** and NAD^+ are shown as yellow and grey sticks, respectively. Panel B. Electron density map SA-omit (2mFo-DFc) of **3a**, in grey, contoured at 1 sigma. Panel C. Superimposition between electron density map of **3a** SA-omit (2mFo-DFc), in grey, and **3a** 2mFo-DFc, in blue.

Figure 2. Stick representations of the possible docking poses of compound **3a** into the binding site of ALDH1A3 (PDB code: 6S6W).

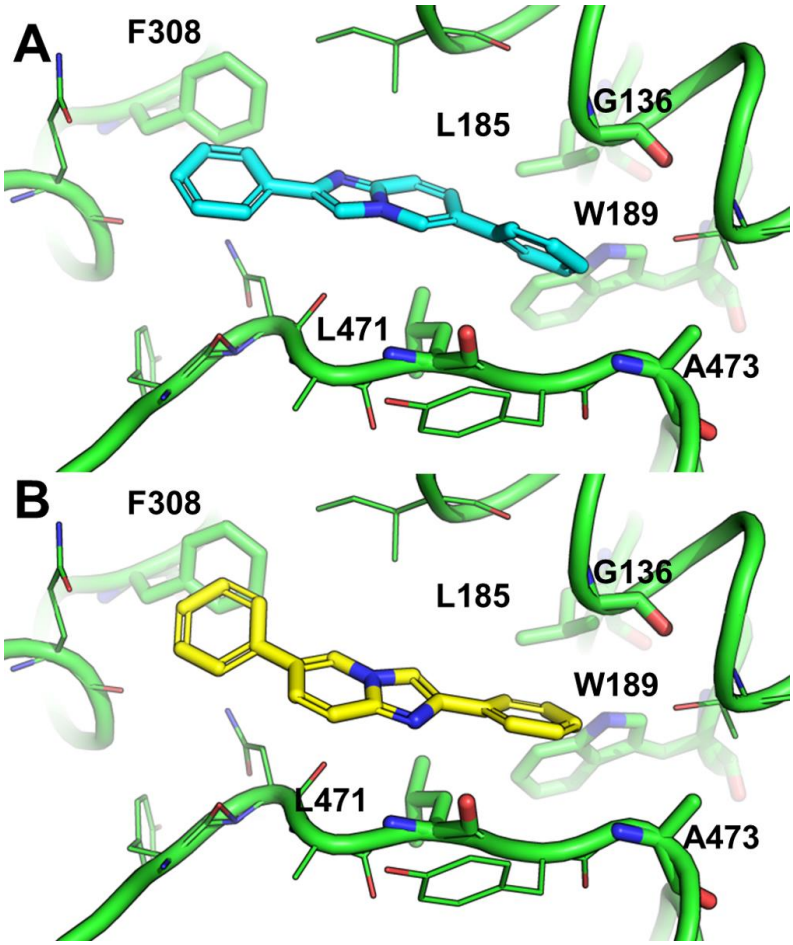

The binding site of ALDH1A3 is represented as green ribbons. Residues relevant for the inhibitor binding have been labelled, and their side chains are shown as green sticks.

Piecing together the inspection of the electron density map of the **3a**-ALDH1A3 complex with the evidences achieved by the molecular modeling study, we resolved to ascribe to **3a** the binding pose depicted in Figure 3. In this conformation, the N1 atom of the scaffold interacts with the carbonyl oxygen of F131, while the whole heterocyclic core lies in a conserved hydrophobic pocket located at the entrance of the tunnel that provides substrate access to and product release from, the catalytic cysteine. Moreover, the phenyl ring in position 6 of the nucleus establishes contacts with the protein backbone, including π-π stacking interaction with W189 (3.8 Å) and Van der Waals contacts with G136 (3.6 Å), L185 (3.8 Å) and L471 (4.5 Å) (Figure 3).

Figure 3. Representation of the main interactions between **3a** and the ALDH1A3 binding site (PDB code: 6S6W).

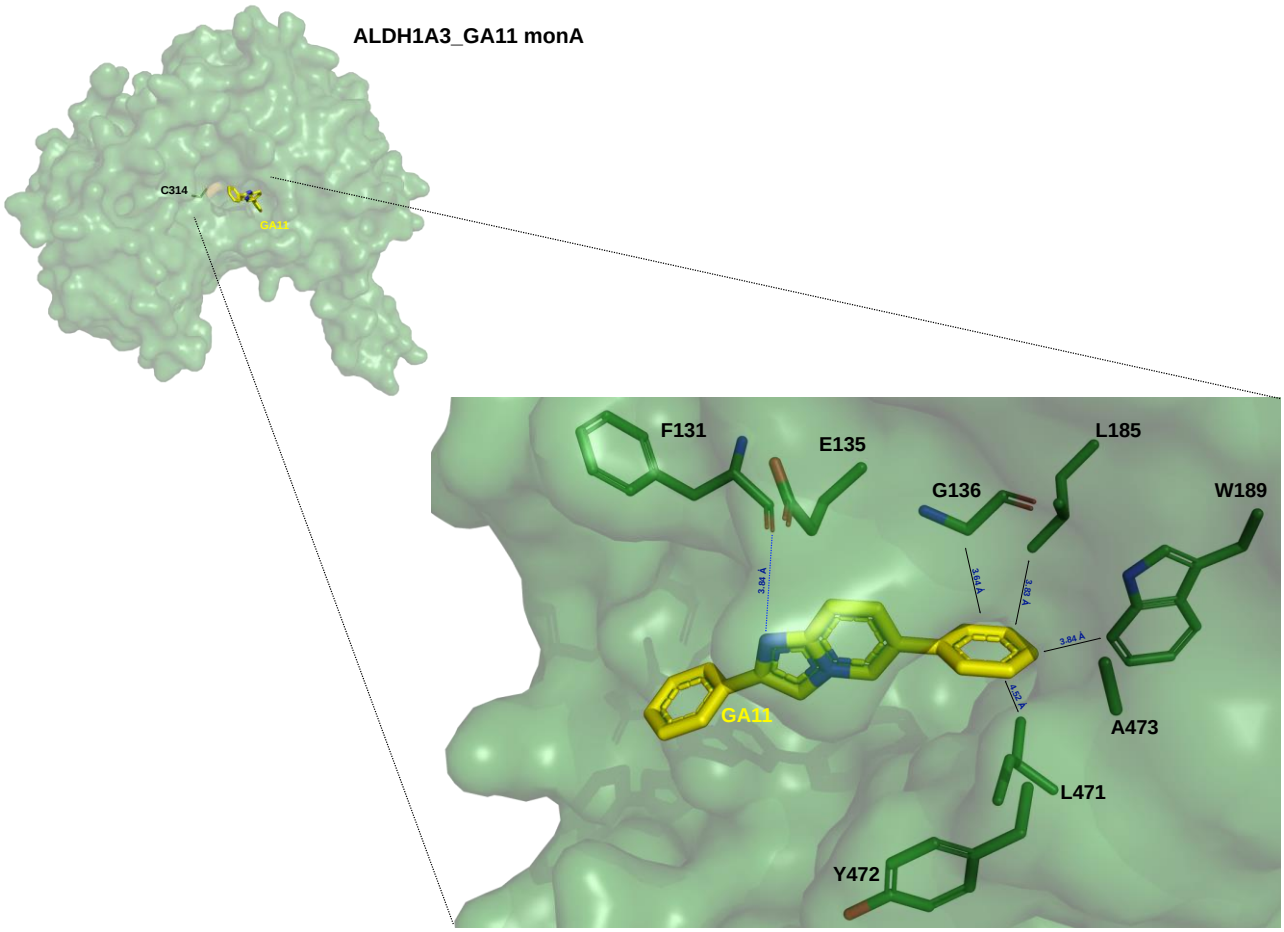

Buried surface areas of monomer A is colored in forest green and the ligand **3a** is shown as yellow stick. Side chains of key residues, involved in **3a** binding, are shown in forest green sticks. E135, F131, G136, L185, W189, A473, L471 and Y472 stabilize through π-π stacking and hydrophobic interactions the **3a** phenyl rings. The carbonyl oxygen of F131 make a hydrogen bond interaction with N1 of **3a**.

The mentioned residues are conserved in each of the 1A1, 1A2 and 1A3 isozymes, being this enzymatic area the one stabilizing retinoic acid binding in the whole members of the 1A subfamily, as demonstrated in a previous work.[14] ALDH1A3 shows a high homology degree compared to the other members of the 1A subfamily. Actually, the 1A3 structure can be optimally superimposed onto human ALDH1A1 (PDB: 4WB9[16]), with a r.m.s.d. of 0.96 Å, and onto human ALDH1A2 (PDB: 6B5G[17]), with a r.m.s.d. of 0.92 Å, based on 485 equivalent Cα–pairs (Figure 4).

Figure 4. Superposition of ALDH1A binding-sites conformations.

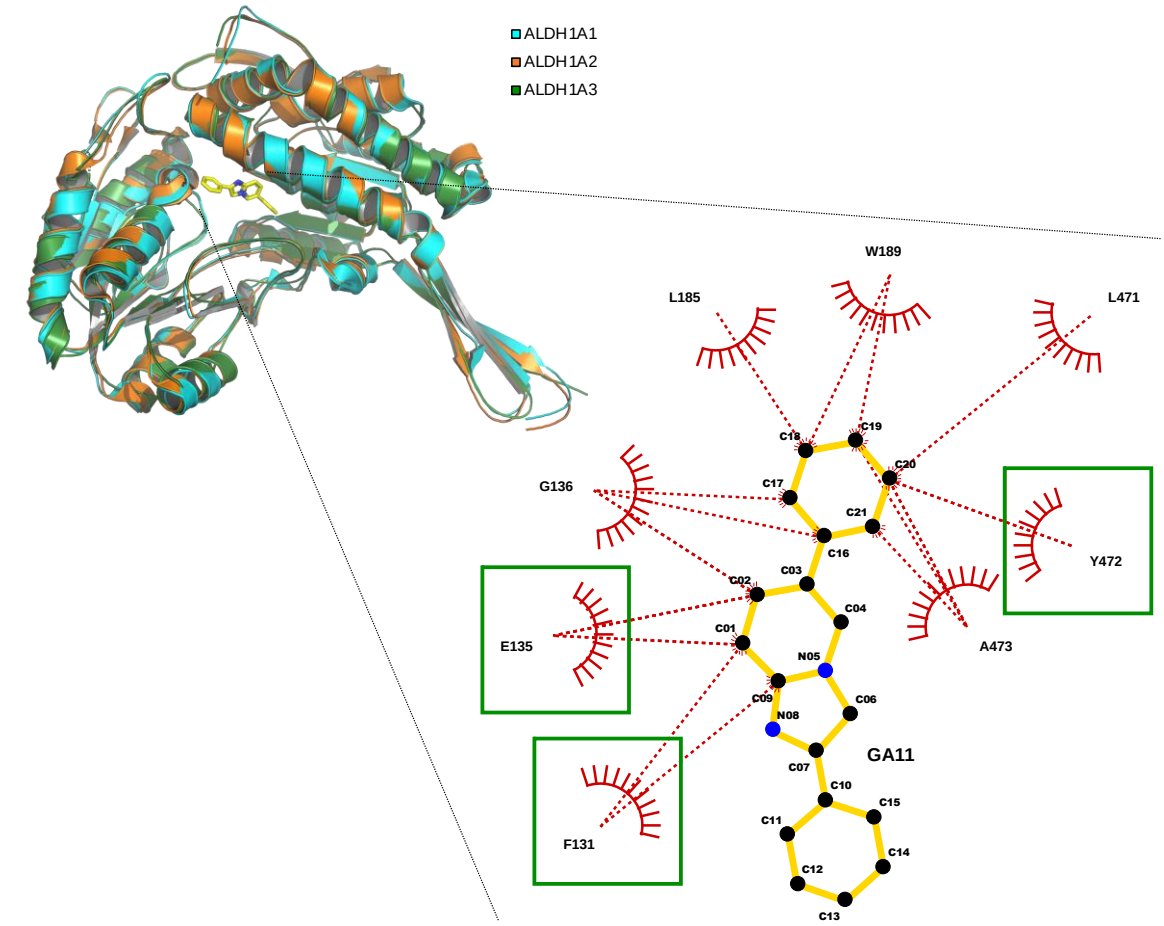

Superposition ribbon representation of monomer overall structures of ALDH1A3 in forest green (PDB code: 6S6W), ALDH1A2 in orange (PDB code: 6B5g), and ALDH1A1 in cyan (PDB code: 4WB9). The three structures maintain the same arrangement. The LigPlus representation of the complex **3a**-ALDH1A3 monomer A, highlights all the eight amino acids involved in **3a** binding site. The ALDH1A3 amino acid residues circled in green are not conserved in ALDH1A1 and ALDH1A2.

In addition, ALDH1A3 shares 71% amino acid identity with human isozymes 1A1 and 72% amino acid identity with 1A2. However, as detailed in Figure 5, a few differences in the amino acid sequences of the three isozymes do exist. Indeed, the superposition of 1A3, 1A1 and 1A2 forms highlights that three amino acids are not conserved. The hydrophilic F131 of ALDH1A3 corresponds to L120 in ALDH1A1 and Y137 in ALDH1A2, the E135 residue of ALDH1A3

corresponds to A124 in ALDH1A1 and Q141 in ALDH1A2, while the Y472 residue of ALDH1A3 corresponds to S461 in ALDH1A1 and to N478 in ALDH1A2. The three mentioned residues affect in particular the binding pocket hosting **3a**, thus giving reason to the inhibitory selectivity displayed by the compound against the three isozymes (Table 2).

Figure 5. Superposition overview of different amino acids involved in **3a**-ALDH1A3 binding.

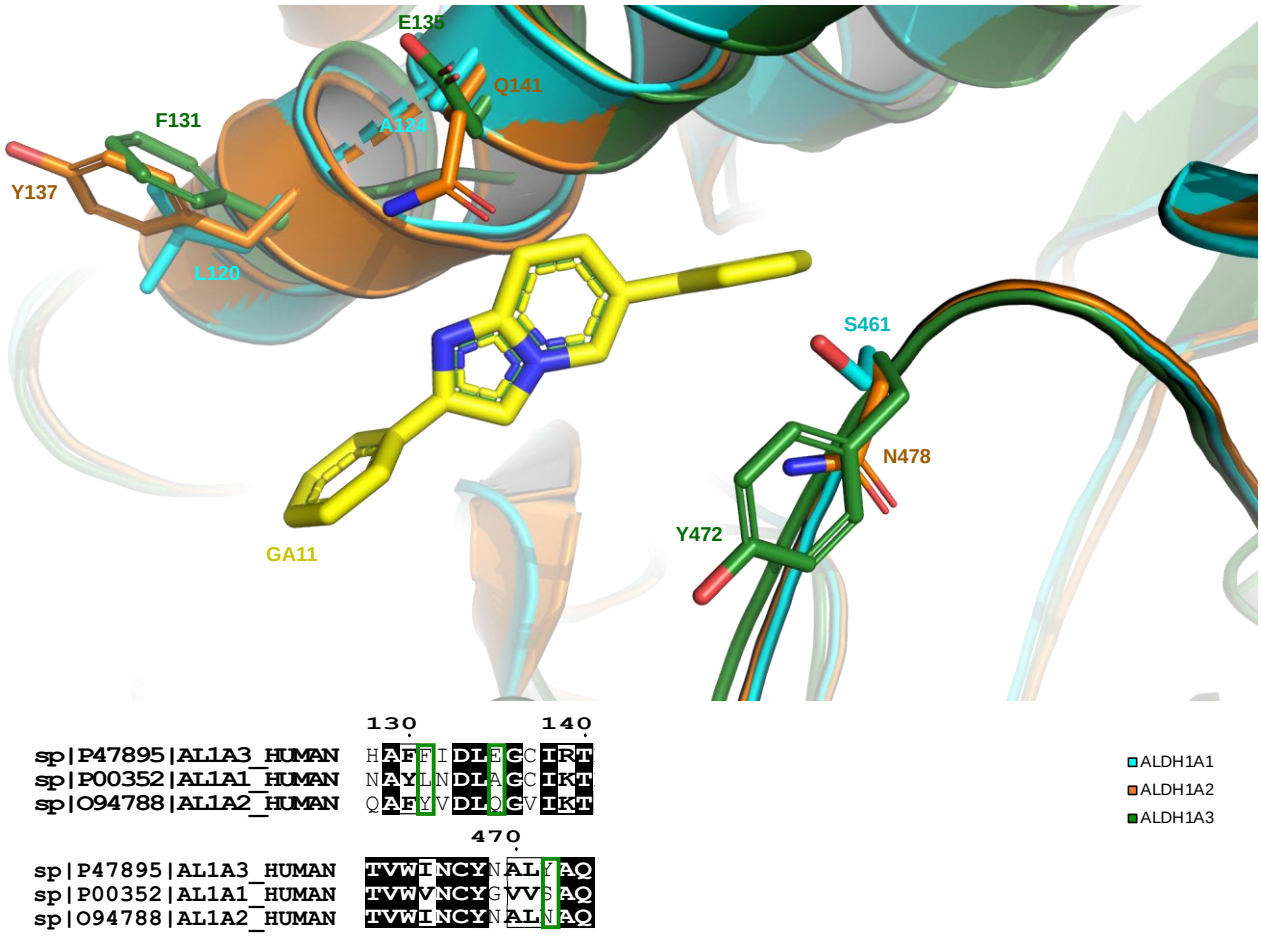

Side chains of key residues involved in the binding (F131, E135, Y472, PDB code: 6S6W) are shown in forest green sticks. The correspondent not conserved residues of ALDH1A2 (Y137, Q141, N478, PDB code: 6B5G) and of ALDH1A1 (L120, A124, S461, PDB code: 4WB9) are represented in orange sticks and cyan sticks, respectively. In the sequence overlapping of the three isoenzymes, the not conserved residues are circled in green.

Overall, both crystallographic studies and molecular modeling investigations evidence that **3a** is able to bind the entrance of the catalytic site of ALDH1A3, without protruding inside the catalytic

pocket. Clear docking sites for phenyl rings in positions 2- and 6- of the nucleus were identified, thus offering interesting clues for the rational optimization of the hit. In particular, they lead to speculate that the insertion of suitable substituents on the two pendant rings may help to fill in further the binding pocket of the target proteins, thus getting to novel effective analogues. On the basis of these premises, we synthesized a number of 6-substituted-imidazo[1,2-*a*]pyridines, **3a-v** (Schemes 1 and 2) as well as few examples of 7-substituted-imidazo[1,2-*a*]pyridines, **7a-i** (Scheme 3), to shed light on both electronic and geometrical requirements of the imidazo[1,2-*a*]pyridine class for the obtainment of ALDH1A3 inhibitors.

Chemistry. The synthesis of the 6-substituted-imidazo[1,2-*a*]pyridines **3a-k,p-v** was performed as outlined in Scheme 1. The commercially available 2-amino-5-bromo pyridine **1** was treated with the suitably substituted 2-bromo-1-phenylethan-1-one, in the presence of potassium carbonate, to achieve the corresponding 2-phenyl-imidazo[1,2-*a*]pyridines **2a-e**. Coupling the obtained heterocycles with differently substituted phenylboronic acids, performed in the presence of $Pd(OAc)_2$ and PPh_3 as the catalysts, provided the desired inhibitors. Compounds **3l,m** were synthesized following the alternative synthetic sequence described in Scheme 2, which allowed to get to the imidazo[1,2-*a*]pyridine derivatives with comparable yields. Coupling 2-amino-5-bromopyridine **1** with the appropriate phenylboronic acids, under the experimental conditions outlined above, gave the intermediate 5-(4-chlorophenyl)pyridin-2-amine **4**, which was cyclized to the desired 2-phenyl-imidazo[1,2-*a*]pyrimidines **3l,m** by reaction with 2-bromo-1-phenylethan-1-one. 7-Substituted-imidazo[1,2-*a*]pyridines, **7a-i**, represented in Scheme 3, were obtained following similar reactions. The commercially available 2-amino-4-bromo pyridine **5** and the appropriate 2-bromo-1-phenylethan-1-ones gave the key intermediates 7-bromo-2-phenylimidazo[1,2-*a*]pyridines **6a-c**, which were converted into the target inhibitors **7a-i** by reaction with different phenyl boronic acids, under the customary coupling conditions in the presence of $Pd(OAc)_2$ and PPh_3 as the catalysts.

Scheme 1. Synthesis of 6-Substituted-imidazo[1,2-*a*]pyridine Derivatives **3a-k,n-v**.

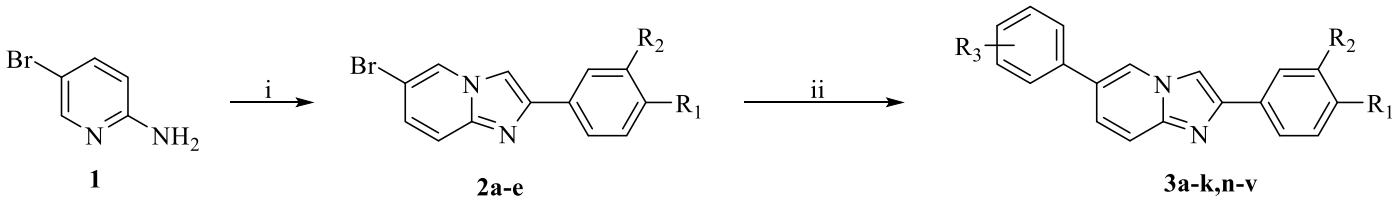

1 **2a-e** **3a-k,n-v**

a: R_1=H, R_2=H
b: R_1=CH_3, R_2=H
c: R_1=OCH_3, R_2=H
d: R_1=NO_2, R_2=H
e R_1=H, R_2=OCH_3

a: R_1=H, R_2=H, R_3=H
b: R_1=H, R_2=H, R_3=4-F
c: R_1=H, R_2=H, R_3=4-Cl
d: R_1=H, R_2=H, R_3=4-SCH_3
e: R_1=H, R_2=H, R_3=4-OCH_3
f: R_1=H, R_2=H, R_3=4-$COOCH_3$
g: R_1=H, R_2=H, R_3=2-CN
h: R_1=H, R_2=H, R_3=3-CN
i: R_1=H, R_2=H, R_3=4-CN
j: R_1=CH_3, R_2=H, R_3=H

k: R_1=OCH_3, R_2=H, R_3=H
n: R_1=NO_2, R_2=H, R_3=4-Cl
o: R_1=OCH_3, R_2=H, R_3=4-OCH_3
p: R_1=OCH_3, R_2=H, R_3=3,4-diOCH_3
q: R_1=OCH_3, R_2=H, R_3=3,5-diOCH_3
r: R_1=CH_3, R_2=H, R_3=4-F
s: R_1=CH_3, R_2=H, R_3=4-Cl
t: R_1=H, R_2=OCH_3, R_3=H
u: R_1=H, R_2=OCH_3, R_3=4-F
v: R_1=H, R_2=OCH_3, R_3=4-Cl

Reagents and conditions:
i) 2-bromo-1-(4-(3)substitutedphenyl)ethan-1-one, K_2CO_3, Δ; ii) Substitued-phenylboronic acid, $Pd(OAc)_2$, PPh_3, K_2CO_3, Δ.

Scheme 2. Synthesis of 6-Substituted-imidazo[1,2-*a*]pyridine Derivatives **3l,m**.

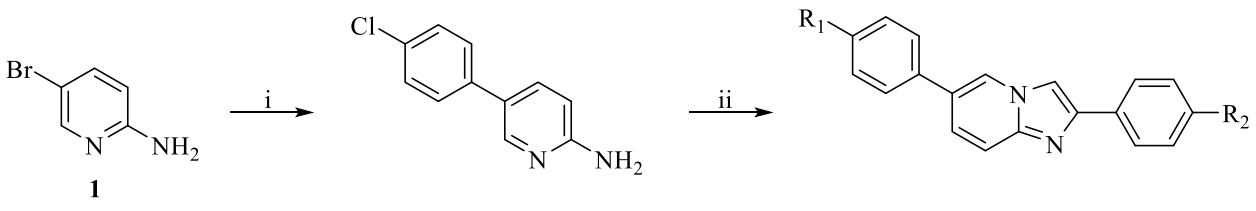

l: R_1=Cl, R_2=Cl
m: R_1=Cl, R_2=Br

Reagents and conditions:
i) 4-Chlorophenylboronic acid, $Pd(OAc)_2$, PPh_3, K_2CO_3, Δ; 2-Bromo-1-(4-substitutedphenyl)ethan-1-one, K_2CO_3, Δ.

Scheme 3. Synthesis of 7-Substituted-imidazo[1,2-*a*]pyridine Derivatives **7a-i.**

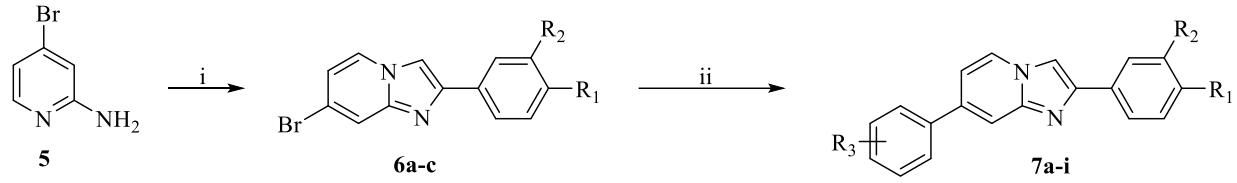

a: R_1=H, R_2=H
b: R_1=CH_3, R_2=H
c: R_1=H, R_2=OCH_3

a: R_1=H, R_2=H, R_3=H
b: R_1=H, R_2=H, R_3=4-F
c: R_1=H, R_2=H, R_3=4-Cl
d: R_1=CH_3, R_2=H, R_3=H
e: R_1=CH_3, R_2=H, R_3=4-F
f: R_1=CH_3, R_2=H, R_3=4-Cl
g: R_1=H, R_2=OCH_3, R_3=H
h: R_1=H, R_2=OCH_3, R_3=4-F
i: R_1=H, R_2=OCH_3, R_3=4-Cl

Reagents and conditions:
i) 2-bromo-1-(4-(3)substitutedphenyl)ethan-1-one, K_2CO_3, Δ; ii) Substitued-phenylboronic acid, $Pd(OAc)_2$, PPh_3, K_2CO_3, Δ.

Functional evaluation and modeling studies. The novel 6-phenyl-substituted-imidazo[1,2-*a*]pyridine derivatives were tested for both their inhibitory efficacy against the human recombinant ALDH1A3 and selectivity towards the ALDH1A1 and ALDH1A2 isoforms. The kinetic parameters were determined for all the compounds, following the experimental protocol described hereafter. Regarding the reference hit **3a** (GA11, IC_{50} 4.7±1.7 μM, Table 2), an in depth analysis of its

functional activity revealed a K_i value of 0.54±0.11 μM and a partially competitive mode of action against the target enzyme ALDH1A3 (Figure 1-SI, Supporting Information). These results are consistent with structural data, showing that the compound binds to the entrance of the catalytic tunnel, hindering partially the substrate flow without coordinating directly the catalytic residue C314. To provide atomistic insights into the mechanism of inhibition, the co-presence of **3a** and the substrate acetaldehyde in the catalytic cavity of ALDH1A3 was investigated by molecular docking and molecular dynamic (MD) simulations (Figure 6). By referring to the crystallographic complex between ALDH1A3 and **3a**, two poses for acetaldehyde were found, i.e. in proximity of F308 and close to C314 (Figure 6A). MD simulations on both docking poses clearly showed that, starting from F308, acetaldehyde quickly leaves the catalytic site and moves to the bulk solvent (Figure 6B). In contrast, starting from C314, acetaldehyde persists within the catalytic tunnel for around 150 ns (Figure 6C) before moving to the bulk solvent, being **3a** firmly anchored at the entrance of the site. Overall, the structural analysis suggests that both acetaldehyde and **3a** can occupy simultaneously the ALDH1A3 catalytic site, thus giving rise to a partially competitive mechanism of action.

Figure 6. Predicted binding mode and MD simulations of acetaldehyde in the **3a**-ALDH1A3 crystallographic complex (PDB code: 6S6W).

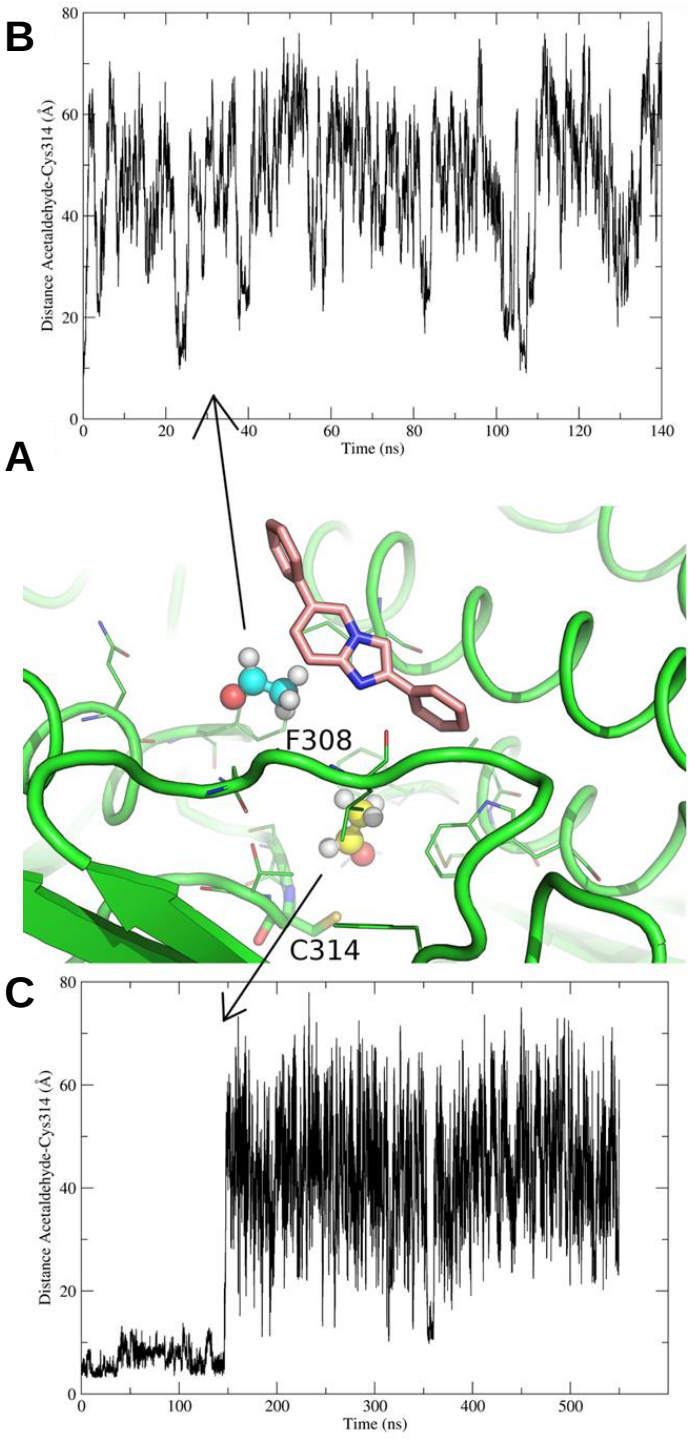

Panel A: obtained docking poses of acetaldehyde, represented as sticks and either cyan or yellow balls. Panels B and C: plots of the distances between acetaldehyde and the catalytic C314 along MD trajectories starting from the docking poses, represented in cyan and yellow respectively, indicated by black arrows. MD simulations on the cyan pose were stopped after around 150 ns, as the small molecule detaches from the ALDH1A3 catalytic site and moves to the bulk solvent.

As for the novel imidazo[1,2-*a*]pyridine derivatives, most of them proved to inhibit the target ALDH1A3 isoform when tested at 25 μM concentration, displaying different degrees of efficacy depending on the substitution patterns on the pendant phenyl rings (Figure 2-SI, Supporting Information). Compounds showing good inhibitory activity at 25 μM were investigated further, to determine their IC_{50} values (Table 2). Results obtained enable us to draft structure-activity relationships for the imidazo[1,2-*a*]pyridine class.

Table 2. ALDH Inhibitory activity of Selected Imidazo[1,2-*a*]pyridine Derivatives **3a-v**.

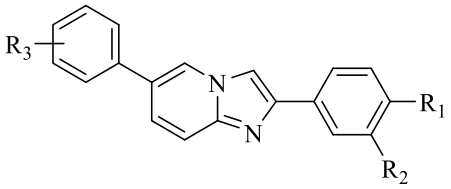

				IC_{50} (μM[a]) or % Inhibition[b]		
N	**R_1**	**R_2**	**R_3**	**ALDH1A1**	**ALDH1A2**	**ALDH1A3**
3a	H	H	H	19.6±1.6	54.6±1.9	4.7±1.7
3b	H	H	4-F	n.a.[c]	n.a.[c]	22.8±1.6
3c	H	H	4-Cl	68.8±1.5	n.a.[c]	45.8±1.7
3d	H	H	4-SCH_3	n.a.[c]	n.a.[c]	27.1±1.5
3e	H	H	4-OCH_3	n.a.[c]	n.a.[c]	17.8±1.5
3f	H	H	4-$COOCH_3$	96.9±2.2	n.a.[c]	27.4±1.6
3h	H	H	3-CN	11.3%	n.a.[c]	5.3±1.5
3i	H	H	4-CN	15.9%	n.a.[c]	5.2±1.7
3j	CH_3	H	H	22.4%	n.a.[c]	11.3±1.5
3m	Br	H	4-Cl	17.3±1.6	n.a.[c]	n.a.[c]
3o	OCH_3	H	4-OCH_3	22.9%	n.a.[c]	11.4±1.6
3p	OCH_3	H	3,4-diOCH_3	17.5%	n.a.[c]	8.3±1.2
3q	OCH_3	H	3,5-diOCH_3	197.7±3.0	n.a.[c]	3.5±1.2
3r	CH_3	H	4-F	n.a.[c]	n.a.[c]	92.9±1.8
3u	H	OCH_3	4-F	n.a.[c]	n.a.[c]	21.2±1.7
3v	H	OCH_3	4-Cl	n.a.[c]	n.a.[c]	6.4±1.3

[a]IC_{50} values represent the concentration required to produce 50% enzyme inhibition.[b]Percentage of enzyme inhibition. Standard errors of the means (SEMs) ≤ 10 %. [c]Not active. No significant enzyme inhibition was observed at 25 μM.

In particular, starting from the unsubstituted hit **3a** (GA11, IC_{50} 4.7±1.7 μM), modifications of the 6-phenyl area alone, through the insertion of increasingly bulky substituents as in compounds **3b-i**, were well tolerated, regardless the electronic properties of the added groups. The best results were achieved with compounds **3h**,**i**, bearing the electro-withdrawing nitrile group in position *meta* and *para* of the ring, respectively, which turned out to be as potent as the parent hit **3a** (**3h**, IC_{50} 5.3±1.5 μM; **3i**, IC_{50} 5.2±1.7 μM). The inhibitory efficacy of the hit was kept unaltered also by inserting a methyl group in position *para* of the 2-phenyl ring, as in derivative **3j** (IC_{50} 11.3±1.5 μM).

Double substitution patterns on both the pendant phenyl rings of the hit were explored as well, pursuing different combinations of both electron-withdrawing and electron-donating substituents. In this regard, the best results in terms of inhibitory efficacy were obtained by using the electron-donating methoxy group. Actually, by merging the 2-(4-methoxy)phenyl residue with a mono- or di-methoxy substitution on the 6-phenyl ring, a relevant activity was obtained and the resulting compounds, **3o-q**, displayed IC_{50} values in the low micromolar range.

Co-crystallizing **3q** (IC_{50} 3.5±1.2 μM) with the human ALDH1A3 enzyme (PDB code: 6TE5, PDB deposition name LQ43, Figure 7), it has been possible to verify that the oxygen atom in position para on the 2-phenyl ring is involved in a hydrogen bond with Q304. This interaction is complemented by a further hydrogen bond between the methoxy group in position *meta* of the 6-phenyl ring (O2) and the NE1 residue of W189 (3.5 Å) and OG1 of T140 (3.39 Å), which ties firmly the compound into the ALDH1A3 binding site. The 6-phenyl ring of the compound establishes also hydrophobic contacts with the protein backbone, including π-π stacking interaction with E135 and Y472, crucial residues of ALDH1A3 not conserved in the parent isoenzymes. Actually, as highlighted in Figure 5, the key Y472 is replaced by S461 and N478 in the 1A1 and 1A2 isoenzymes, respectively, thus accounting for the inhibitory selectivity displayed by **3q** (Table 2).

Figure 7. Overall monomer structure of human ALDH1A3 in complex with **3q** (PDB code: 6TE5, PDB deposition name LQ43).

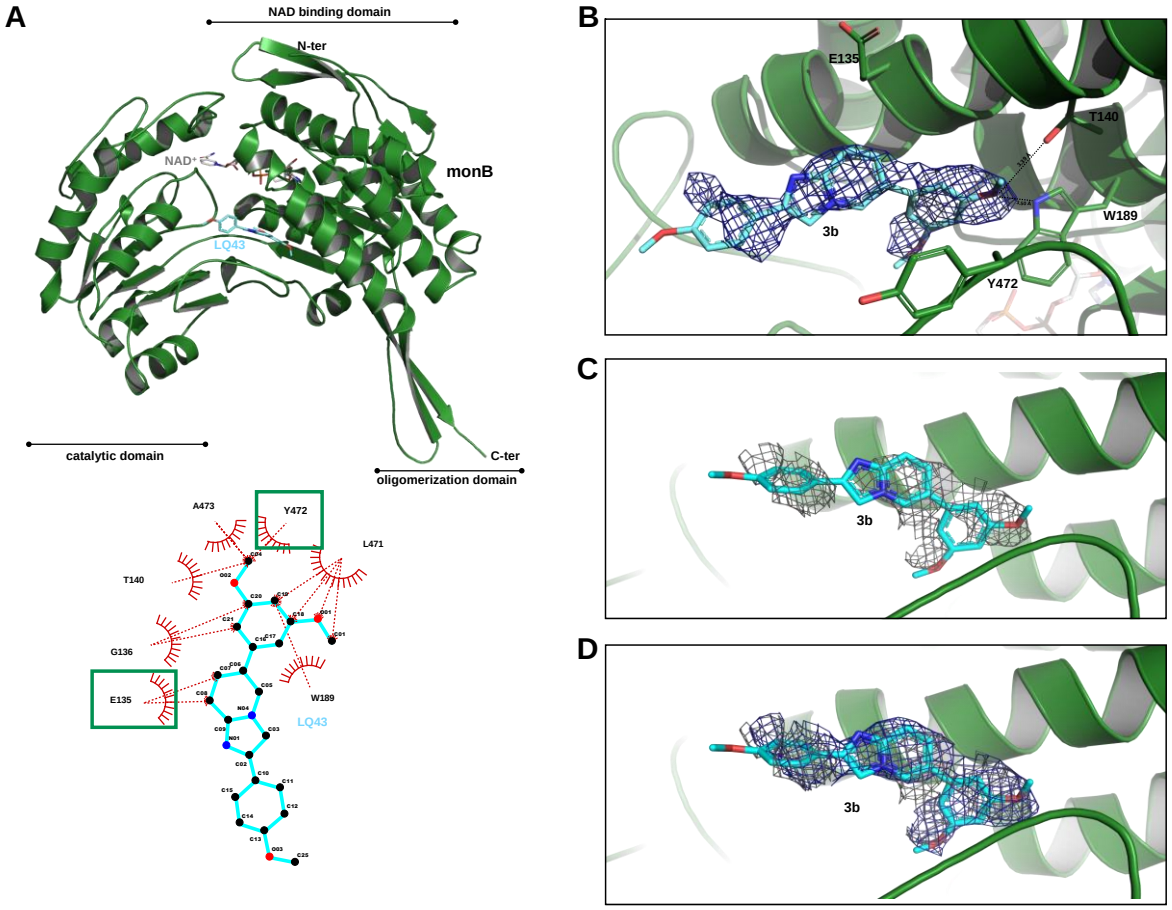

Panel A. Ribbon representation of the overall structure of the monomer of ALDH1A3. The LigPlus representation of the complex **3q**-ALDH1A3 monomer B highlights all the amino acids involved in the binding. The ALDH1A3 amino acid residues circled in green are not conserved in ALDH1A1 and ALDH1A2. Panel B. Compound **3q** into the enzyme binding site. The ligand is shown as cyan stick and the side chains of key residues, involved in the binding, are shown in forest green sticks. The electron density map (2mFo-dFc) countered at 1.0 sigma, used to determine the presence of **3q** into the enzyme binding site, is in blue. Panel C. Electron density map SA-omit (2mFo-dFc) of **3q**, in grey, contoured at 1 sigma. Panel D. Superimposition between electron density map of **3q** SA-omit (2mFo-dFc), in grey, and **3q** 2mFo-dFc, in blue.

The same order of efficacy was also obtained with compounds **3u** (IC_{50} 21.1±1.7 μM) and **3v** (IC_{50} 6.4±1.3 μM), bearing a 2-(3-methoxy)phenyl fragment combined with a fluoro and a chloro atom, respectively, in the *para* position of the 6-phenyl ring (Table 2).

Tested against the related dehydrogenase isoforms ALDH1A1 and ALDH1A2, none of the synthesized compounds but the unsubstituted **3a** showed any relevant inhibitory efficacy (Figure 2-SI, Supporting Information), thus proving that suitably amending the aromatic tails of the imidazo[1,2-*a*]pyridine core a complete selectivity between similar enzymes can be achieved. However, it is worth mentioning derivative **3m**, 2-(4-bromophenyl)-6-(4-chlorophenyl)imidazo[1,2-*a*]pyridine, whose double substitutions carried out with a 4-bromo and a 4-chloro on the 2- and 6-phenyl ring, respectively, turned upside down the activity profile of the imidazopyridine class proving to be fully selective for the ALDH1A1 subtype (IC_{50} 17.3±1.6 μM).

To verify that the 2,6-diphenyl motif is the structural geometry that best comply with the structural requirements of the ALDH1A3 binding site, the series of **7a-i** analogues was synthesized and tested as well. Shifting the phenyl ring to position 7 of the imidazopyridine nucleus modified significantly the inhibitory activity of the resulting compounds, which was substantially downsized against the ALDH1A3 isoform and even nullified in the case of ALDH1A1 and ALDH1A2 enzymes (Figure 3-SI, Supporting Information).

Anti-proliferative activity. Representative examples of the imidazopyridine derivatives, **3b**-**c**,**f**,**v**, chosen among those possessing the best profile of inhibitory activity and selectivity, were tested for their anti-proliferative efficacy against three different patient-derived glioma sphere samples, both proneural (PN-157) and mesenchymal (MES-267 and MES-374) ones, already characterized for their ALDH1 expression patterns.[11,12] The 72-hour exposure to the test compounds significantly inhibited the growth of glioma spheres. All the tested imidazopyridines displayed IC_{50} values in the nanomolar/sub-nanomolar range against the different cell subtypes, showing a more marked activity against the MES-374 line (Table 3). The 6-(4-fluoro)phenyl derivative **3b**, combining the best functional profile in terms of activity and selectivity against the ALDH1 proteins (Table 2)

confirmed its efficacy also in the cell-based test, showing IC_{50} values of 25.2 nM, 63.4 nM, and 2.58 pM against the PN-157, MES-267, and MES-374 cell lines, respectively.

Table 3. Anti-proliferative Activity of Selected Imidazo[1,2-*a*]pyridine Derivatives **3a-c**,**e,f,u,v** against 157-, 267-, and 374-GSC lines.

	GSC Lines		
N	**157 (IC_{50}, nM[a])**	**267 (IC_{50}, nM[a])**	**374 (IC_{50}, nM[a])**
3a	151.0	46.9	2.74
3b	25.2	63.4	0.00258
3c	53.1	21.5	0.0196
3e	2660	660	n.t.[b]
3f	822.0	823.0	n.t[b]
3u	1510	350	n.t.[b]
3v	29.6	71.2	13.5

[a]IC_{50} values represent the concentration of drug that decreased cell count by 50%. Standard errors of the means (SEMs) ≤ 10%. [b]N.t.: not tested.

Concluding Remarks

In this work we described a novel series of 2,6-diphenyl-imidazo[1,2-*a*]pyridine derivatives as aldehyde dehydrogenase inhibitors, proving their significance not only as pharmacological tools but also as promising functional leads. Moving from the previously described hit GA11[12] and taking advantage of both crystallographic studies and molecular modeling investigations, we succeeded in customizing the selectivity profile of the compound by varying its substitution pattern on both the pendant phenyl rings. A 2-(4-bromophenyl)-6-(4-chlorophenyl) decoration, as in derivative **3m**, gave a compound fully selective for the ALDH1A1 isoenzyme, while most of the other explored substituents led to compounds able to inhibit the key ALDH1A3 subtype, accountable for GBM stem cells vitality being involved in the differentiation of progenitor cells into mature entities. In

this respect, derivative **3b** turned out to be the most promising one. Besides showing the most efficient combination of inhibitory activity against the target 1A3 isoenzyme and selectivity towards the parent 1A1 and 1A2, **3b** displayed a relevant anti-proliferative efficacy when tested against well-characterized patient-derived glioma sphere samples, showing IC_{50} values in the nanomolar/picomolar range. This compound represents therefore an original example of ALDH inhibitor whose functional profile may provide, in principle, a novel and viable chance to treat GBM by targeting stem-like cells. Clearly, thorough investigations in animal models of GBM are now necessary, to prove its robustness as a novel prototype of drug candidate.

Experimental Section

Chemistry. Melting points were determined using a Reichert Köfler hot-stage apparatus and are uncorrected. Routine ^{1}H-NMR and ^{13}C-NMR spectra were recorded in DMSO-d_6 solution on a Bruker 400 spectrometer operating at 400 MHz. Evaporation was performed in vacuo (rotary evaporator). Analytical TLCs were carried out on Merck 0.2 mm precoated silica gel aluminium sheets (60 F-254). Purity of the target inhibitors was determined by HPLC analysis, using a Merck Hitachi D-7000 liquid chromatograph (PDA, 250-500 nm) and a Luna® C18 column (250 mm x 4.6 mm, 5 μm, Phenomenex), with a gradient of 30% water and 70% acetonitrile and a flow rate of 1.0 mL/min. All the compounds showed percent purity values ≥95% (Figures 4-SI to 18-SI, Supporting Information). 4-Bromopyridin-2-amine, 5-bromopyridin-2-amine, the suitably substituted 2-bromo-1-phenylethan-1-one, and the appropriate boronic acids, used to obtain the target inhibitors, were from Alfa Aesar, Aldrich and Fluka. 6-Bromo-2-phenylimidazo[1,2-*a*]pyridine **2a**,[18] 6-bromo-2-(p-tolyl)imidazo[1,2-*a*]pyridine **2b**,[18] 6-bromo-2-(4-methoxyphenyl)imidazo[1,2-a]pyridine **2c**,[18] 5-(4-chlorophenyl)pyridin-2-amine **4**,[19] were synthesized following reported procedures.

General Procedure for the Synthesis of 6-bromo-2-(substituted)phenylimidazo[1,2-*a*]pyridines, 2d,e. A solution of 5-bromopyridin-2-amine **1** (1.00 mmol) in ethanol was added with

the suitably substituted 2-bromo-1-phenylethan-1-one (1.00 mmol) and potassium carbonate (138 mg, 1.00 mmol), and the resulting mixture was refluxed under stirring until the disappearance of the starting material (TLC analysis). After cooling, the crude obtained was evaporated to dryness, then water was added to the residue and the desired heterocycle, **2d,e**, separated as a white solid, was collected by filtration, purified through recrystallization from the suitable solvent and characterized with physio-chemical and spectroscopic data.

6-Bromo-2-(4-nitrophenyl)imidazo[1,2-*a*]pyridine, **2d**. White solid. M.p. 258-260 °C. Cryst. solvent: Acetonitrile. Yield: 55%. ^{1}H-NMR (δ, ppm): 8.953 (d, 1H, J=1.20 Hz), 8.603 (s, 1H), 8.321 (d, 2H, J = 8.88 Hz), 8.242 (d, 2H, J = 8.88 Hz), 7.638 (d, 1H, J = 9.60 Hz), 7.445 (dd, 1H, J = 9.60 Hz, J= 1.71 Hz).

6-Bromo-2-(3-methoxyphenyl)imidazo[1,2-*a*]pyridine, **2e**. White solid. M.p. 232-234 °C. Cryst. solvent: EtOH. Yield: 76%. ^{1}H-NMR (δ, ppm): 9.189 (s, 1H), 8.678 (s, 1H), 7.928 (d, 1H, J = 9.28 Hz), 7.853 (d, 1H, J = 9.44 Hz), 7.557 (s, 1H), 7.550 (d, 1H, J = 7.95 Hz), 7.499 (t, J = 8.09 Hz, 1H), 7.091 (d, 1H, J = 7.92 Hz), 3.867 (s, 3H).

General Procedure for the Synthesis of 2,6-(substituted)diphenylimidazo[1,2-*a*]pyridines, 3a-k,n-v. A solution of the appropriate imidazo[1,2-*a*]pyridine derivative **2a-e** (1.00 mmol), $Pd(OAc)_2$ (0.10 mmol) and PPh_3 (0.20 mmol) in toluene was added with the suitable phenyl boronic acid (1.50 mmol), dissolved in ethanol, and 2 mL of Na_2CO_3 2M. The resulting mixture was refluxed under stirring until the disappearance of the starting material (TLC analysis). After cooling, the crude obtained was evaporated to dryness and the residue was purified by column chromatography (silica gel, ethyl acetate/petroleum ether). The pure product was then recrystallized from the suitable solvent and characterized by physio-chemical and spectroscopic data.

2,6-Diphenylimidazo[1,2-*a*]pyridine, **3a**. White solid. M.p. 179-181 °C. Cryst. solvent: MeOH. Yield: 78%. ^{1}H-NMR (δ, ppm): 8.899 (s, 1H), 8.420 (s, 1H), 7.999 (d, 2H, J = 7.10 Hz), 7.755 (d, 2H, J = 7.20 Hz), 7.679 (d, 1H, J = 9.40 Hz), 7.615 (dd, 1H, J = 9.40 Hz, J = 1.80 Hz), 7.524 (t, 2H, J = 7.40 Hz), 7.466 (t, 3H, J = 7.44 Hz), 7.441 (t, 1H, J = 7.32 Hz), 7.343 (t, 1H, J = 7.30 Hz). ^{13}C-

NMR (δ, ppm): 145.45, 144.66, 137.14, 134.32, 129.57, 129.20, 128.24, 128.18, 126.99, 126.07, 125.70, 125.41, 124.47, 117.12, 110.02.

6-(4-Fluorophenyl)-2-phenylimidazo[1,2-*a*]pyridine, **3b**. White solid. M.p. 173-175 °C. Cryst. solvent: AcOEt. Yield: 58%. ^{1}H-NMR (δ, ppm): 8.879 (s, 1H), 8.405 (s, 1H), 8.002 (d, 2H, J = 7.70 Hz), 7.786 (dd, 2H, J = 7.10 Hz, J = 5.36 Hz), 7.679 (d, 1H, J = 9.16 Hz), 7.595 (dd, 1H, J = 9.38 Hz, J = 1.86 Hz), 7.463 (t, 2H, J = 6.78 Hz), 7.358 (t, 3H, J = 8.33 Hz). ^{13}C-NMR (δ, ppm): 163.64, 161.21, 145.40, 144.55, 136.92, 134.17, 133.60, 133.57, 129.22, 129.09, 129.01, 128.31, 126.05, 125.46, 124.83, 124.45, 117.06, 116.51, 116.29, 114.84, 110.05.

6-(4-Chlorophenyl)-2-phenylimidazo[1,2-*a*]pyridine, **3c**. White solid. M.p. 192-194 °C. Cryst. solvent: MeOH. Yield: 56%. ^{1}H-NMR (δ, ppm): 8.934 (s, 1H), 8.413 (s, 1H), 8.004 (d, 2H, J = 7.08 Hz), 7.779 (d, 2H, J = 8.60 Hz), 7.690 (d, 1H, J = 9.36 Hz), 7.614 (dd, 1H, J = 9.44 Hz, J = 1.88 Hz), 7.582 (d, 2H, J = 8.61 Hz), 7.466 (t, 2H, J = 7.62 Hz), 7.345 (t, 1H, J = 7.37 Hz). ^{13}C-NMR (δ, ppm): 145.54, 144.62, 136.03, 134.23, 129.52, 129.21, 128.74, 128.29, 126.08, 125.13, 124.73, 124.44, 117.19, 110.08.

6-(4-(Methylthio)phenyl)-2-phenylimidazo[1,2-*a*]pyridine, **3d**. White solid. M.p. 158-160 °C. Cryst. solvent: Acetonitrile. Yield: %. ^{1}H-NMR (δ, ppm): 8.873 (s, 1H), 8.394 (s, 1H), 7.990 (d, 2H, J = 7.32 Hz), 7.678 (d, 2H, J = 8.30), 7.590 (d, 2H, J = 7.60 Hz), 7.493-7.329 (m, 5H), 3. 603 (s, 3H). ^{13}C-NMR (δ, ppm): 145.39, 144.58, 138.37, 134.30, 133.56, 129.20, 128.24, 127.37, 126.95, 126.05, 125.18, 125.11, 124.09, 117.12, 109.99, 15.13.

6-(4-Methoxyphenyl)-2-phenylimidazo[1,2-*a*]pyridine, **3e**. White solid. M.p. 173-175 °C. Cryst. solvent: EtOH. Yield: %. ^{1}H-NMR (δ, ppm): 8.765 (s, 1H), 8.369 (s, 1H), 7.944 (d, 2H, J = 7.81 Hz), 7.631 (d, 4H, J = 8.78), 7.444 (t, 2H, J = 6.84 Hz), 7.327 (t, 1H, 6.35), 7.047 (d, 2H, J = 7.32 Hz), 3. 809 (s, 3H). ^{13}C-NMR (δ, ppm): 159.56, 145.14, 144.42, 134.27, 129.37, 129.20, 128.15, 126.03, 125.52, 123.63, 116.96, 115.03, 109.92, 55.71.

Methyl 4-(2-phenylimidazo[1,2-*a*]pyridin-6-yl)benzoate, **3f**. White solid. M.p. 165-168 °C. Cryst. solvent: EtOH. Yield: %. ^{1}H-NMR (δ, ppm): 9.014 (s, 1H), 8.413 (s, 1H), 8.063 (d, 2H, J = 8.30 Hz), 7.994 (d, 2H, J = 8.31), 7.889 (d, 2H, J = 8.30 Hz), 7.454 (t, 2H, 6.83), 7.328 (t, 1H, J = 7.32 Hz), 3.875 (s, 3H). ^{13}C-NMR (δ, ppm): 166.52, 166.40, 145.16, 143.74, 139.29, 130.35, 130.31, 130.27. 130.23, 129.74, 129.57, 128.91, 128.88, 127.81, 127.78, 127.45, 127.43, 61.33, 52.71, 52.62, 14.64.

2-(2-Phenylimidazo[1,2-*a*]pyridin-6-yl)benzonitrile, **3g**. White solid. M.p. 213-215 °C. Cryst. solvent: EtOH. Yield: 26%. ^{1}H-NMR (δ, ppm): 8.857 (s, 1H), 8.855 (s, 1H), 8.852 (d, 3H, J = 7.76 Hz), 7.879 (t, 1H, J = 7.64), 7.775-7.740 (m, 2H), 7.655 (t, 1H, J = 7.68 Hz), 7.475 (t, 3H, J = 7.72 Hz), 7.355 (t, 1H, J = 7.37 Hz). ^{13}C-NMR (δ, ppm): 145.85, 144.56, 141.31, 134.36, 134.15, 134.09, 130.81, 129.24, 129.16, 128.43, 126.88, 126.55, 126.16, 123.44, 118.80, 116.94, 111.19, 110.24.

3-(2-Phenylimidazo[1,2-*a*]pyridin-6-yl)benzonitrile, **3h**. White solid. M.p. 170-171 °C. Cryst. solvent: EtOH. Yield: 30%. ^{1}H-NMR (δ, ppm): 9.043 (s, 1H), 8.415 (s, 1H), 8.272 (s, 1H), 8.110 (d, 1H, J = 8.00 Hz), 8.022 (d, 2H, J = 7.30 Hz), 7.881 (d, 1H, J = 7.80), 7.737 (d, 2H, J = 7.77), 7.707 (s, 1H), 7.470 (t, 2H, J = 7.52), 7.352 (t, 1H, J = 7.28). ^{13}C-NMR (δ, ppm): 145.71, 144.68, 138.36, 134.12, 131.69, 130.72, 130.54, 129.20, 128.36, 126.14, 125.44, 125.00, 123.67, 119.18, 117.23, 112.69, 110.12.

4-(2-Phenylimidazo[1,2-*a*]pyridin-6-yl)benzonitrile, **3i**. White solid. M.p. 209-210 °C. Cryst. solvent: Acetonitrile. Yield: 39%. ^{1}H-NMR (δ, ppm): 9.066 (s, 1H), 8.436 (s, 1H), 8.017 (d, 2H, J = 7.08), 7.979 (d, 4H, J = 10.20 Hz), 7.729 (d, 1H, J = 9.37 Hz), 7.690 (dd, 1H, J = 10.16, Hz, J = 1.60 Hz), 7.472 (t, 2H, J = 7.60 Hz), 7.354 (t, 1H, J = 7.40). ^{13}C-NMR (δ, ppm): 145.81, 144.75, 141.83, 134.10, 133.46, 129.23, 128.40, 127.76, 125.84, 124.91, 119.26, 117.33, 110.67, 110.25.

6-Phenyl-2-(p-tolyl)imidazo[1,2-*a*]pyridine, **3j**. White solid. M.p. 165-167 °C. Cryst. solvent: Acetonitrile. Yield: 36%. ^{1}H-NMR (δ, ppm): 8.879 (s, 1H), 8.359 (s, 1H), 7.887 (d, 2H, J = 8.01

Hz), 7.739 (d, 2H, J = 7.33 Hz), 7.663 (d, 1H, J = 9.29 Hz), 7.603 (dd, 1H, J = 9.36 Hz, J = 1.76 Hz), 7.520 (t, 2H, J = 7.58 Hz), 7.415 (t, 1H, J = 7.37 Hz), 7.272 (d, 2H, J = 8.09 Hz), 2.353 (s, 3H). ^{13}C-NMR (δ, ppm): 159.62, 145.38, 144.49, 137.19, 134.52, 130.44, 129.57, 128.14, 127.79, 127.41, 126.97, 126.82, 125.58, 125.21, 124.34, 116.79, 114.67, 108.97, 55.64.

2-(4-Methoxyphenyl)-6-phenylimidazo[1,2-*a*]pyridine, **3k**. White solid. M.p. 176-179 °C. Cryst. solvent: EtOH. Yield: %. ^{1}H-NMR (δ, ppm): 8.879 (s, 1H), 8.359 (s, 1H), 7.887 (d, 2H, J = 8.01 Hz), 7.739 (d, 2H, J = 7.33 Hz), 7.662 (d, 1H, J = 9.29 Hz), 7.603 (dd, 1H, J = 9.36, Hz, J = 1.76 Hz), 7.521 (t, 2H, J = 7.40 Hz), 7.415 (t, 1H, J = 7.37 Hz), 7.272 (d, 2H, J = 8.09 Hz). ^{13}C-NMR (δ, ppm): 145.57, 144.57, 137.54, 137.17, 131.54, 129.78, 129.56, 128.15, 126.96, 126.00, 125.58, 125.23, 124.38, 117.00, 109.55, 21.34.

6-(4-Chlorophenyl)-2-(4-nitrophenyl)imidazo[1,2-*a*]pyridine, **3n**. White solid. M.p. 198-200 °C. Cryst. solvent: EtOH. Yield: 28%. ^{1}H-NMR (δ, ppm): 8.957 (s, 1H), 8.644 (s, 1H), 8.324 (d, 2H, J = 8.88 Hz), 8.270 (d, 2H, J = 8.89 Hz), 7.789 (d, 2H, J= 8.52 Hz), 7.736 (d, 1H, J = 9.37 Hz), 7.677 (dd, 1H, J = 9.40 Hz, J= 1.56 Hz), 7.588 (d, 2H, J = 8.48 Hz). ^{13}C-NMR (δ, ppm): 146.92, 144.96, 143.08, 140.72, 135.69, 133.17, 129.48, 128.74, 126.77, 126.03, 124.94, 124.54, 117.47, 112.54.

2,6-Bis(4-methoxyphenyl)imidazo[1,2-*a*]pyridine, **3o**. White solid. M.p. 202-203 °C. Cryst. solvent: EtOH. Yield: %. ^{1}H-NMR (δ, ppm): 8.767 (s, 1H), 8.257 (s, 1H), 7.899 (d, 2H, J = 6.84 Hz), 7.644 (d, 2H, J = 6.84 Hz), 7.566 (d, 2H, J = 6.84 Hz), 7.052 (d, 2H, J = 7.08 Hz), 7,006 (d, 2H, J = 7.08 Hz), 3.794 (s, 6H). ^{13}C-NMR (δ, ppm): 159.54, 145.19, 144.29, 133.76, 132.48, 131.91, 129.28, 128.13, 126.82, 125.24, 123.51, 116.66, 115.03, 114.66, 108.87, 55.72, 55.63.

6-(3,4-Dimethoxyphenyl)-2-(4-methoxyphenyl)imidazo[1,2-*a*]pyridine, **3p**. White solid. M.p. 245-248 °C. Cryst. solvent: EtOH. Yield: %. ^{1}H-NMR (δ, ppm): 8.805 (s, 1H), 8.259 (s, 1H), 7.806 (d, 2H, J = 8.79 Hz), 7.580 (s, 1H) 7.567 (d, 1H, J = 7.37 Hz), 7.20 (d, 2H, J = 8.06 Hz), 7.039 (d, 1H, J = 7.56 Hz), 6.998 (d, 2H, J = 8.55 Hz), 3.865 (s, 3H), 3.796 (s, 6H). ^{13}C-NMR (δ, ppm):

159.52, 149.67, 149.12, 145.37, 144.45, 129.83, 127.34, 126.99, 125.53, 125.26, 123.63, 119.16, 116.64, 114.62, 112.74, 110.74, 108.75, 56.12, 56.06, 55.60.

6-(3,5-Dimethoxyphenyl)-2-(4-methoxyphenyl)imidazo[1,2-*a*]pyridine, **3q**. White solid. M.p. 213-215 °C. Cryst. solvent: EtOH. Yield: %. ^{1}H-NMR (δ, ppm): 9.176 (s, 1H), 8.553 (s, 1H), 8.136 (d, 1H, J = 9.45 Hz), 7.934 (d, 2H, J = 8.84 Hz), 7.903 (d, 1H, J = 9.56 Hz), 7.171 (d, 2H, J = 8.76 Hz), 6.945 (s, 1H), 6.939 (s, 1H), 6.637 (s, 1H), 3.858 (s, 9H). ^{13}C-NMR (δ, ppm): 161.47, 159.57, 145.52, 144.66, 139.28, 127.38, 126.89, 125.38, 125.21, 124.59, 116.65, 114.64, 109.87, 105.11, 100.05, 55.84, 55.62.

6-(4-Fluorophenyl)-2-(p-tolyl)imidazo[1,2-*a*]pyridine, **3r**. White solid. M.p. 156-158 °C. Cryst. solvent: Acetonitrile. Yield: 39%. ^{1}H-NMR (δ, ppm): 8.862 (s, 1H), 8.348 (s, 1H), 7.888 (d, 2H, J = 8.09 Hz), 7.781 (dd, 2H, J = 7.76 Hz, J = 4.36 Hz), 7.656 (d, 1H, J = 9.41 Hz), 7.580 (dd, 1H, J = 9.37 Hz, J = 1.80 Hz), 7.356 (t, 2H, J = 8.87 Hz), 7.270 (d, 2H, J = 7.43 Hz), 2.351 (s, 3H). ^{13}C-NMR (δ, ppm): 163.62, 161.19, 145.60, 144.48, 137.54, 133.67, 133.64, 131.51, 129.76, 129.04, 128.96, 126.00, 125.18, 124.65, 124.36, 116.98, 116.46, 116.25, 109.54, 21.32.

6-(4-Chlorophenyl)-2-(p-tolyl)imidazo[1,2-*a*]pyridine, **3s**. White solid. M.p. 188-190 °C. Cryst. solvent: Acetonitrile. Yield: 36%. ^{1}H-NMR (δ, ppm): 8.914 (s, 1H), 8.353 (s, 1H), 7.889 (d, 2H, J = 8.09 Hz), 7.775 (d, 2H, J = 8.56 Hz), 7.660 (d, 1H, J = 9.32 Hz), 7.597 (dd, 1H, J = 9.12 Hz, J = 1.80 Hz), 7.577 (d, 2H, J = 8.53 Hz), 7.271 (d, 2H, J = 8.01 Hz), 2.352 (s, 3H). ^{13}C-NMR (δ, ppm): 145.67, 144.54, 137.60, 136.06, 132.97, 131.46, 129.78, 129.50, 128.72, 126.02, 124.95, 124.63, 124.32, 117.06, 109.61, 21.34.

2-(3-Methoxyphenyl)-6-phenylimidazo[1,2-*a*]pyridine, **3t**. White solid. M.p. 140-141 °C. Cryst. solvent: Acetonitrile. Yield: 39%. ^{1}H-NMR (δ, ppm): 8.877 (s, 1H), 8.433 (s, 1H), 7.741 (d, 2H, J = 7.24 Hz), 7.690 (d, 1H, J = 9.36 Hz), 7.618 (dd, 1H, J = 9.36 Hz, J = 1.76 Hz), 7.574 (s, 1H), 7.560 (d, 1H, J = 7.42), 7.522 (t, 2H, J = 7.44 Hz), 7.418 (t, 1H, J = 7.37), 7.370 (t, 1H, J = 8.20 Hz), 6.912 (dd, 1H, J = 7.91 Hz, J = 1.76 Hz), 3.845 (s, 3H). ^{13}C-NMR (δ, ppm): 160.13, 145.38, 144.52,

136.02, 135.64, 133.02, 130.29, 129.52, 128.77, 125.18, 124.70, 124.48, 118.49, 117.20, 114.15, 111.15, 110.38, 55.57.

6-(4-Fluorophenyl)-2-(3-methoxyphenyl)imidazo[1,2-*a*]pyridine, **3u**. White solid. M.p. 147-148 °C. Cryst. solvent: Acetonitrile. Yield: 27%. ^{1}H-NMR (δ, ppm): 8.865 (s, 1H), 8.424 (s, 1H), 7.785 (dd, 2H, J = 9.00 Hz, J = 5.78 Hz), 7.686 (d, 1H, J = 9.24 Hz), 7.587-7.564 (m, 3H), 7.391-7.337 (m, 3H), 6.916 (d, 1H, J = 9.40 Hz), 3.845 (s, 3H). ^{13}C-NMR (δ, ppm): 163.65, 161.21, 160.13, 145.30, 144.45, 135.69, 133.63, 133.60, 130.27, 129.10, 129.01, 125.41, 124.80, 124.43, 118.47, 117.11, 116.49, 116.28, 114.10, 111.14, 110.31, 55.55.

6-(4-Chlorophenyl)-2-(3-methoxyphenyl)imidazo[1,2-*a*]pyridine, **3v**. White solid. M.p. 161-163 °C. Cryst. solvent: MeOH. Yield: 24%. ^{1}H-NMR (δ, ppm): 8.911 (s, 1H), 8.426 (s, 1H), 7.777 (d, 2H, J = 6.64 Hz), 7.693 (d, 1H, J = 9.36 Hz), 7.610 (dd, 1H, J = 9.44 Hz, J = 1.76 Hz), 7.371 (t, 1H, J = 8.10 Hz), 7.915 (dd, 1H, J = 6.00 Hz, J = 0.40 Hz), 3.844 (s, 3H). ^{13}C-NMR (δ, ppm): 160.14, 145.39, 144.52, 136.03, 135.65, 133.02, 130.29, 129.52, 128.76, 125.18, 124.70, 124.49, 118.50, 117.20, 114.15, 111.17, 110.37, 55.58.

Synthesis of 2,6-bis(4-chlorophenyl)imidazo[1,2-a]pyridine, 3l, and 2-(4-bromophenyl)-6-(4-chlorophenyl)imidazo[1,2-a]pyridine, 3m. A solution of 5-(4-chlorophenyl)pyridin-2-amine[19] **4** (1.00 mmol) in ethanol was added with the suitably substituted 2-bromo-1-phenylethan-1-one (1.00 mmol) and potassium carbonate (138 mg, 1.00 mmol), and the resulting mixture was refluxed under stirring until the disappearance of the starting material (TLC analysis). After cooling, the crude obtained was evaporated to dryness, then water was added to the residue and the desired heterocycle **3l,m**, separated as a white solid, was collected by filtration, purified through recrystallization from the suitable solvent and characterized with physio-chemical and spectroscopic data.

2,6-Bis(4-chlorophenyl)imidazo[1,2-*a*]pyridine, **3l**. White solid. M.p. 278-280 °C. Cryst. solvent: EtOH. Yield: 81%. ^{1}H-NMR (δ, ppm): 9.192 (s, 1H), 8.692 (s, 1H), 8.102 (s, 1H), 8.031 (d, 2H, J = 8.60 Hz), 7.945 (d, 1H, J = 8.90 Hz), 7.842 (d, 2H, J = 8.50 Hz), 7.686-7.638 (m, 4H). ^{13}C-NMR (δ,

ppm): 140.58, 136.55, 135.27, 134.26, 134.20, 132.39, 129.97, 129.81, 129.29, 128.61, 128.47, 126.70, 126.58, 113.28, 112.19.

2-(4-Bromophenyl)-6-(4-chlorophenyl)imidazo[1,2-*a*]pyridine, **3m**. White solid. M.p. 298-300 °C. Cryst. solvent: MeOH. Yield: 48%. ^{1}H-NMR (δ, ppm): 9.183 (s, 1H), 8.693 (s, 1H), 8.096 (d, 1H, J = 8.16 Hz), 7.976-7.926 (m, 3H), 7.841 (d, 2H, J = 8.60 Hz), 7.807 (d, 2H, J = 8.50 Hz), 7.640 (d, 2H, J = 8.60 Hz). ^{13}C-NMR (δ, ppm): 140.50, 136.45, 134.29, 134.14, 132.88, 132.52, 129.80, 129.27, 128.67, 126.91, 126.58, 124.05, 113.18, 112.21.

General Procedure for the Synthesis of 7-bromo-2-(substituted)phenylimidazo[1,2-*a*]pyridines, 6a-c. A solution of 4-bromopyridin-2-amine **5** (1.00 mmol) in ethanol was added with the suitably substituted 2-bromo-1-phenylethan-1-one (1.00 mmol) and potassium carbonate (138 mg, 1.00 mmol), and the resulting mixture was refluxed under stirring until the disappearance of the starting material (TLC analysis). After cooling, the crude obtained was evaporated to dryness, then water was added to the residue and the desired heterocycle, **6a-c**, separated as a white solid, was collected by filtration, purified through recrystallization from the suitable solvent and characterized with physio-chemical and spectroscopic data.

7-Bromo-2-phenylimidazo[1,2-*a*]pyridine, **6a**. White solid. M.p. 290 °C, dec. Cryst. solvent: MeOH. Yield: 81%. ^{1}H-NMR (δ, ppm): 8.732 (d, 1H, J = 7.25 Hz), 8.695 (s, 1H), 8.151 (s, 1H), 7.958 (d, 2H, J = 7.05 Hz), 7.565 (d, 1H, J = 7.22 Hz), 7.514 (t, 3H, J = 7.12 Hz).

7-Bromo-2-(p-tolyl)imidazo[1,2-*a*]pyridine, **6b**. White solid. M.p. 280 °C, dec. Cryst. solvent: EtOH. Yield: 83%. ^{1}H-NMR (δ, ppm): 8.747 (d, 1H, J = 7.12 Hz), 8.675 (s, 1H), 8.156 (s, 1H), 7.848 (d, 2H, J = 8.16 Hz), 7.568 (d, 1H, J = 7.07 Hz), 7.399 (d, 2H, J = 8.00 Hz), 2.390 (s, 3H).

7-Bromo-2-(3-methoxyphenyl)imidazo[1,2-*a*]pyridine, **6c**. White solid. M.p. 261-263 °C. Cryst. solvent: MeOH. Yield: 70%. ^{1}H-NMR (δ, ppm): 8.605 (d, 1H, J = 7.15 Hz), 8.581 (s, 1H), 8.049 (s, 1H), 7.538-7.521 (m, 2H), 7.480-7.429 (m, 2H), 7.027 (d, 1H, J = 7.09 Hz), 3.854 (s, 3H).

General Procedure for the Synthesis of 2,7-(substituted)diphenylimidazo[1,2-*a*]pyridines, 7a-i. A solution of the appropriate imidazo[1,2-*a*]pyridine derivative **6a-c** (1.00 mmol), $Pd(OAc)_2$ (0.10

mmol) and PPh_3 (0.20 mmol) in toluene was added with the suitable phenyl boronic acid (1.50 mmol), dissolved in ethanol, and 2 mL of Na_2CO_3 2M. The resulting mixture was refluxed under stirring until the disappearance of the starting material (TLC analysis). After cooling, the crude obtained was evaporated to dryness and the residue was purified by column chromatography (silica gel, ethyl acetate/petroleum ether). The pure product was then recrystallized from the suitable solvent and characterized by physio-chemical and spectroscopic data.

2,7-Diphenylimidazo[1,2-*a*]pyridine, **7a**. White solid. M.p. 196-198 °C. Cryst. solvent: MeOH. Yield: 45%. ^{1}H-NMR (δ, ppm): 8.611 (d, 1H, J = 7.10 Hz), 8.435 (s, 1H), 8.004 (d, 2H, J = 7.04 Hz), 7.924 (s, 1H), 7.851 (d, 2H, J = 7.20 Hz), 7.522 (t, 2H, J = 7.54 Hz,), 7.465 (t, 2H, J = 7.40 Hz), 7.431 (t, 1H, J = 7.58), 7.360 (t, 1H, J = 7.33 Hz,), 7.310 (dd, 1H, J = 7.12 Hz, J = 1.84 Hz,). ^{13}C-NMR (δ, ppm): 145.45, 144.66, 137.14, 134.32, 129.57, 129.20, 128.24, 128.18, 126.99, 126.07, 125.70, 125.41, 124.47, 117.12, 110.02.

7-(4-Fluorophenyl)-2-phenylimidazo[1,2-*a*]pyridine, **7b**. White solid. M.p. 222-223 °C. Cryst. solvent: MeOH. Yield: 42%. ^{1}H-NMR (δ, ppm): 8.606 (d, 1H, J = 7.24 Hz), 8.427 (s, 1H), 7.999 (d, 2H, J = 7.36 Hz,), 7.910 (s, 1H), 7.901 (t, 2H, J = 5.40 Hz), 7.464 (t, 2H, J = 7.66 Hz,), 7.360 (d, 2H, J = 7.56 Hz), 7.342 (t, 1H, J = 7.33 Hz), 7.294 (dd, 1H, J = 7.14 Hz, J = 1.78 Hz). ^{13}C-NMR (δ, ppm): 163.65, 161.21, 145.45, 144.54, 134.26, 133.64, 133.61, 129.20, 129.09, 129.01, 128.26, 126.07, 125.39, 124.77, 124.48, 117.11, 116.50, 116.28, 110.01.

7-(4-Chlorophenyl)-2-phenylimidazo[1,2-*a*]pyridine, **7c**. White solid. M.p. 224-226 °C. Cryst. solvent: Acetonitrile. Yield: 35%. ^{1}H-NMR (δ, ppm): 8.617 (d, 1H, J = 7.14 Hz,), 8.442 (s, 1H), 8.003 (d, 2H, J = 7.08 Hz), 7.959 (s, 1H), 7.888 (d, 2H, J = 6.65 Hz,), 7.565 (d, 2H, J = 6.65 Hz,), 7.466 (t, 2H, J = 7.60 Hz), 7.344 (t, 1H, J = 7.37 Hz), 7.307 (dd, 1H, J = 7.12 Hz, J = 1.88 Hz). ^{13}C-NMR (δ, ppm): 145.84, 145.64, 137.22, 135.49, 134.29, 133.48, 129.49, 129.22, 128.78, 128.29, 127.48, 126.05, 113.59, 111.75, 109.57.

7-Phenyl-2-(p-tolyl)imidazo[1,2-*a*]pyridine, **7d**. White solid. M.p. 251-252 °C. Cryst. solvent: EtOH. Yield: 30%. ^{1}H-NMR (δ, ppm): 8.590 (d, 1H, J = 7.12 Hz), 8.374 (s, 1H), 7.886 (d, 3H, J = 8.09 Hz), 7.844 (d, 2H, J = 6.09 Hz), 7.518 (t, 2H, J = 7.55 Hz), 7.426 (t, 1H, J = 7.34 Hz), 7.293 (dd, 1H, J = 7.20 Hz, J = 1.88 Hz), 7.269 (d, 2H, J = 7.89 Hz), 2.351 (s, 3H). ^{13}C-NMR (δ, ppm): 145.83, 145.70, 138.41, 137.53, 136.71, 131.60, 129.78, 129.56, 128.66, 127.29, 126.96, 125.98, 113.25, 111.89, 108.96, 21.35.

7-(4-Fluorophenyl)-2-(p-tolyl)imidazo[1,2-*a*]pyridine, **7e**. White solid. M.p. 266-268 °C, dec. Cryst. solvent: Acetonitrile. Yield: 21%. ^{1}H-NMR (δ, ppm): 8.588 (d, 1H, J = 7.12 Hz), 8.371 (s, 1H), 7.915-7.873 (m, 5H), 7.346 (t, 2H, J = 8.85 Hz), 7.291-7.259 (m, 3H), 2,350 (s, 3H). ^{13}C-NMR (δ, ppm): 146.04, 145.42, 137.54, 135.68, 131.58, 129.78, 129.13, 129.05, 127.31, 125.98, 116.48, 116.26, 113.25, 111.81, 108.95, 21.34.

7-(4-Chlorophenyl)-2-(p-tolyl)imidazo[1,2-*a*]pyridine, **7f**. White solid. M.p. 270-275 °C, dec. Cryst. solvent: Acetonitrile. Yield: 27%. ^{1}H-NMR (δ, ppm): 8.597 (d, 1H, J = 7.08 Hz), 8.384 (s, 1H), 7.935 (s, 1H), 7.882 (dd, 4H, J = 8.39 Hz, J = 1.90 Hz), 7.566 (d, 2H, J = 6.66 Hz), 7.299 (dd, 1H, J = 7.20 Hz, J = 1.84 Hz), 7.270 (d, 2H, J = 7.81 Hz), 2.350 (s, 3H). ^{13}C-NMR (δ, ppm): 137.69, 135.41, 133.50, 129.80, 129.49, 128.77, 127.95, 127.46, 125.99, 123.80, 117.94, 116.96, 113.57, 111.67, 109.11, 21.35.

2-(3-Methoxyphenyl)-7-phenylimidazo[1,2-*a*]pyridine, **7g.** White solid. M.p. 176-178 °C. Cryst. solvent: MeOH. Yield: 57%. ^{1}H-NMR (δ, ppm): 8.597 (d, 1H, J = 7.10 Hz), 8.450 (s, 1H), 7.930 (s, 1H), 7.849 (d, 2H, J = 7.82 Hz), 7.568 (s, 1H), 7.538 (d, 1H, J = 7.20 Hz), 7.521 (t, 2H, J = 7.54 Hz), 7.429 (t, 1H, J = 7.31 Hz), 7.369 (t, 1H, J = 8.16 Hz), 7.309 (dd, 1H, J = 7.12 Hz, J = 1.88 Hz), 6.911 (d, 1H, J = 8.22 Hz), 3.845 (s, 3H). ^{13}C-NMR (δ, ppm): 160.13, 145.70, 145.55, 138.37, 136.89, 135.79, 130.28, 129.56, 128.69, 127.36, 126.98, 118.44, 114.11, 113.38, 112.04, 111.08, 109.71, 55.55.

7-(4-Fluorophenyl)-2-(3-methoxyphenyl)imidazo[1,2-*a*]pyridine, **7h.** White solid. M.p. 180-182 °C. Cryst. solvent: Acetonitrile. Yield: 60%. ^{1}H-NMR (δ, ppm): 8.595 (d, 1H, J = 7.20 Hz), 8.446 (s, 1H), 7.930 (s, 1H), 7.916 (d, 1H, J = 8.96 Hz), 7.894 (d, 1H, J = 8.72), 7.575 (s, 1H), 7.565 (d, 1H, J = 7.84), 7.380 (d, 2H, J = 8.08), 7.359 (t, 1H, J = 8.32 Hz), 7.295 (dd, 1H, J = 7.12 Hz, J = 1.80 Hz), 6.911 (d, 1H, J = 8.16 Hz), 3.844 (s, 3H). ^{13}C-NMR (δ, ppm): 163.65, 161.22, 160.13, 145.30, 144.45, 135.69, 133.63, 133.60, 130.28, 129.10, 129.02, 125.42, 124.80, 124.44, 118.47, 117.12, 116.50, 116.28, 114.11, 111.13, 110.31, 55.55.

7-(4-Chlorophenyl)-2-(3-methoxyphenyl)imidazo[1,2-*a*]pyridine, **7i.** White solid. M.p. 182-183 °C. Cryst. solvent: MeOH. Yield: 60%. ^{1}H-NMR (δ, ppm): 8.605 (d, 1H, J = 7.16 Hz), 8.460 (s, 1H), 7.969 (s, 1H), 7.887 (d, 2H, J = 8.61 Hz), 7.569 (d, 4H, J = 7.89 Hz,), 7.371 (t, 1H, J = 8.08 Hz), 7.307 (dd, 1H, J = 7.12 Hz, J = 1.80 Hz), 6.914 (d, 1H, J = 8.10 Hz), 3.844 (s, 3H). ^{13}C-NMR (δ, ppm): 160.12, 145.69, 145.55, 137.20, 135.71, 135.50, 133.49, 130.29, 129.48, 128.77, 127.45, 118.44, 114,15, 113.61, 111.78, 111.10, 109.86, 55.55.

Biology. Materials and Methods.

Expression and purification of human ALDHs. To obtain a large amount of pure ALDH1A1, ALDH1A2 and ALDH1A3 isoenzymes, a common experimental protocol has been optimized for the three proteins. The full-length ALDH1A1, ALDH1A2 and ALDH1A3 expression vectors, were transformed in *E. coli* strain BL21(DE3) (Novagen) spread onto 2xTY agar plates with 50 μg/mL ampicillin for ALDH1A1 and ALDH1A3, and 50 μg/mL kanamicine for ALDH1A2, for overnight growth, at 37 °C. The next day, colonies were scraped and inoculated in 1 L 2xTY medium supplemented with 50 μg/mL ampicillin for ALDH1A1 and ALDH1A3, and 50 μg/mL kanamicine for ALDH1A2. For the three enzymes, once achieved OD_{600} of 0.6–0.8, the temperature was shifted to 20 °C to induce the recombinant protein production. Induced cells, collected by centrifugation, were re-suspended in 1/25 original volume of lysis buffer (50 mM Na_2HPO_4, 300 mM NaCl, 1 mM β-mercaptoethanol, 20 mM imidazole, pH 7.5) and 1 μL per 80 mL lysis buffer of benzonase nuclease (250 U/ μL). Plasma membranes of BL21(DE3) cells were fragmented by applying high

pressure through the use of a French Press, three times at 1.5 KBar. Protease inhibitor cocktail from SIGMA (100 μL per 40 mL lysis buffer) was added to the crude extract that was clarified by 40 minutes centrifugation at 20,000 rpm. The supernatant was purified by a His-tag affinity chromatography followed by size-exclusion chromatography, using an AKTA FPLC system, at 4 °C. To evaluate the purity and homogeneity of the protein, after each purification step, eluted fractions were analyzed by SDS-PAGE and the protein quantification was always determined by Bradford protein assay. In the first purification step, the soluble fraction of recombinant human 6xHis-ALDH1A* was purified with a Qiagen Ni-NTA Superflow 5 mL cartridge. The supernatant was loaded on the Ni-NTA column, previously equilibrated with 10 column volumes of lysis buffer. The Ni-NTA cartridge was washed with 50 mM Na_2HPO_4, 300 mM NaCl, 1 mM β-mercaptoethanol, 50 mM imidazole, pH 7.5, until the absorbance at 280 nm return to the baseline (15 column volumes). The recombinant protein was eluted with 50 mM Na_2HPO_4, 300 mM NaCl, 1 mM β-mercaptoethanol, 250 mM imidazole, pH 8, by applying a linear gradient in 10 column volumes. Eluted fractions were pooled and concentrated to 5 ml with Merck Millipore Amicon Ultra-15 30 kDa and loaded on a HiLoad 16/600 Superdex 200 pg column on AKTA FPLC system. Elution buffer contained 20 mM TrisHCl pH 8.0, 150 mM KCl, 1mM β-mercaptoethanol, and a flow rate of 1 mL/min was applied. This procedure allowed to obtain about 20 mg of pure and active ALDH1A3, ALDH1A2 and ALDH1A1 used for both crystallization trials and kinetic analyses.

High-throughput screening to determine the inhibitory efficacy of imidazo[1,2-*a*]pyridine derivatives. A high throughput screening campaign was performed for enzymes ALDH1A3, ALDH1A1 and ALDH1A2, using the previously reported continuous spectrometric assay for ALDH1A3 optimized to suit Greiner Bio-One® 96- UV-Transparent Microplate.[14] Tests were carried out by using 200 μl of reaction mixture, containing 20 mM Tris HCl pH 8.0, 1 mM β-mercaptoethanol, 150 mM KCl, 15% DMSO 500 μM NAD^+ and 2,6 μM of pure recombinant isoenzymes. Reactions were started by the addition of 20 mM acetaldehyde. Change in absorbance

at 340 nm (ε_{NADH}=6220 M^{-1} cm^{-1}) was monitored for 30 min in a Tecan® Sunrise at 25 °C. The activity of each enzymes was tested in the presence of each synthesized compound at 25 μM concentration, in triplicates.

Enzyme kinetic analysis to calculate IC_{50} values of the most promising compound. Selected compounds showing the best inhibitory activity at 25 μM were investigated further for their inhibitory efficacy, to calculate the IC_{50} values. The enzymatic inhibition assays were performed in a total volume of 200 μl of 20 mM Tris HCl pH 8.0, 1 mM β-mercaptoethanol, 150 mM KCl, 15% DMSO, 500 μM NAD^+, 2,6 μM of pure recombinant isoenzymes in the presence of different inhibitors concentrations from 100 μM to 0.78125 μM and pre-incubated for 5 minutes. The kinetic parameters were determined by fitting the measured data to a Michaelis-Menten curve,[20] by using SigmaPlot.[21]

Crystallization and Structure Determination. Crystals of ALDH1A3 in complex with **3a** (PDB deposition name GA11) and **3q** (PDB deposition name LQ45) were obtained by using the vapour-diffusion technique in sitting drop and applying a spare-matrix-based strategy with a crystallization robot (Oryx4, Douglas Instruments). The best crystals of **3a**-ALDH1A3 were grown by mixing 0.5 μl of protein solution at a concentration of 8 mg/mL, pre-incubated with 1 mM NAD^+ and 300 μM **3a**, with an equal volume of a reservoir solution containing 2.4 M sodium malonate, pH 7.0, and equilibrated against 50 μl of the reservoir solution, at 20 °C in about 30 days. For X-ray data collection, crystals were quickly equilibrated in a solution containing the crystallization buffer and 12.5% glycerol as cryo-protectant and flash frozen at 100 K in liquid nitrogen. Data up to 3.2 Å resolution were collected at the beamline ID29 European Synchrotron Radiation Facility (ESRF, Grenoble, France). Analysis of the diffraction data set allowed us to assign the crystal to the orthorhombic $P2_122_1$ space group with cell dimensions of a = 81.56 Å, b = 89.36 Å, c = 159.04 Å and $\alpha = \beta = \gamma = 90°$, containing two molecules per asymmetric unit with a corresponding solvent content of 52.5%. The best crystals of **3q**-ALDH1A3 were grown by mixing 0.5 μl of protein solution at a concentration of 8 mg/mL, pre-incubated with 1 mM NAD^+ and 300 μM **3q**, with an

equal volume of a reservoir solution containing 2.4 M sodium malonate, pH 7.0, and equilibrated against 50 μl of the reservoir solution, at 20 °C in about 30 days. For X-ray data collection, crystals were quickly equilibrated in a solution containing the crystallization buffer and 12.5% glycerol as cryo-protectant and flash frozen at 100 K in liquid nitrogen. Data up to 3.2 Å resolution were collected at the beamline ID29 European Synchrotron Radiation Facility (ESRF, Grenoble, France). Analysis of the diffraction data set allowed us to assign the crystal to the orthorhombic $P2_122_1$ space group with cell dimensions of a = 81.2 Å, b = 89.4 Å, c = 159.2 Å and $\alpha = \beta = \gamma = 90°$, containing two molecules per asymmetric unit with a corresponding solvent content of 47%. Data were processed using the program package XDS[22] and the CCP4 suite of programs[23] was used for scaling. Determination of both structures, **3a**-ALDH1A3 and **3q**-ALDH1A3, were carried out by means of the molecular replacement technique using the coordinates of the tetramer of human ALDH1A3 as the search model (PDB code 5FHZ[14]). PHASER[24] was used to automatically determine the ALDH1A3 structure in complex with the two compounds. The initial model was subjected to iterative cycles of crystallographic refinement with the programs REFMAC5[25] and PHENIX.REFINE,[26] alternated with manual graphic session for model building using the program Coot.[27] 5% of randomly chosen reflections were excluded from refinement of the structure and used for the Free R factor calculation.[28] The program ARP/wARP[29] was used for adding solvent molecules. Refinement was continued until convergence to R-factor and free R-factor values of 0.19 and 0.26 for **3a**-ALDH1A3 and 0.18 and 0.24 for **3q**-ALDH1A3, respectively, with ideal geometry. Data collection and refinement statistics are given in Table 1. The atomic coordinates and structure factors of human ALDH1A3 in complex with **3a** (PDB deposition name GA11) and **3q** (PDB deposition name LQ43) have been deposited with the Protein Data Bank (www.rcsb.org) with the accession codes 6S6W and 6TE5, respectively.

Illustrations. Figures were generated using the program PyMOL.[30]

Molecular Modeling. The crystallographic structure of ALDH1A3 solved in this work was used as rigid receptor in molecular docking simulations, which were performed with GOLD docking

program version 5.0.1.[31,32] PLP scoring function was used for ranking ligand's poses. The binding site was centered in the mass center of residues Gly136, Trp189, and Leu471 and had a radius of 18 Å. Twenty genetic algorithm runs were carried out and visually inspected.

Anti-proliferative assays on GSCs. The glioma sphere cultures used to investigate the anti-proliferative activity of the novel compounds were generated by I. N. at the University of Alabama at Birmingham, following previously reported procedures.[11,12,33] They were cultured in DMEM/F-12 medium (Invitrogen) containing 2% (vol/vol) B27 supplement (Invitrogen), epidermal growth factor (EGF, 20 ng/ml, Peprotech), basic fibroblast growth factor (bFGF, 20 ng/ml, Peprotech) and heparin (2.5 μg/ml). Cells were dissociated into single cell solution with Accutase and seeded into 96 well plates at 2,000 cells/well, as previously described,[12] then treated for 72h with the test compounds or their vehicles alone. Stock solutions of the test compounds were obtained in DMSO, whose concentration in the final test solutions never exceeded 0.5%. At the end of the experiment, medium was removed and cell viability was measured using the AlamarBlue test (ThermoFischer Scientific), according to manufacturer's protocol. The concentration of compounds able to reduce cell proliferation by 50% (IC_{50}) *vs* controls were calculated with the SPSS 19.0 software by analyzing the nonlinear regression fit of the mean values of the data obtained in triplicate experiments.

Supporting Information Available. Figure 1-SI, showing biochemical characterization of derivative **3a**. Figure 2-SI, showing residual ALDHs activities in the presence of 2,6-disubstituted-imidazo[1,2-*a*]pyridine derivatives **3a-v**, tested at 25 μM. Figure 3-SI, showing residual ALDHs activities in the presence of 2,7-disubstituted-imidazo[1,2-*a*]pyridine derivatives **7a-i**, tested at 25 μM. Figures 4-SI to 18-SI, showing HPLC traces of 2,6-disubstituted-imidazo[1,2-*a*]pyridine derivatives, **3a-v**. Molecular Formula String (CSV).

This material is available free of charge via the Internet at http://pubs.acs.org.

PDB ID Codes. 6S6W for the structure of human ALDH1A3 in complex with compound **3a** (GA11 in the PDB repository); 6TE5 for the structure of human ALDH1A3 in complex with compound **3q** (LQ43 in the PDB repository). Authors will release the atomic coordinates and experimental data upon article publication.

Corresponding Authors Information. S.G., email: silvia.garavaglia@uniunpo.it; C.L.M., email: concettina.lamotta@unipi.it.

Author Contributions. L.Q. and E.G. contributed equally to the work.

Acknowledgement. C.L.M. acknowledges the University of Pisa for the financial support (PRA_2017_51 Project). S.G. acknowledges the University of Piemonte Orientale (grant Ricerca Ateneo FAR_2016) and ROCHE per la ricerca 2017, for the financial support. All the authors thank the ESRF for data collections at the beam lines ID29.

Abbreviations. GBM, glioblastoma multiforme; GSCs, glioma stem-like cells; PN-GSCs, proneural glioma stem-like cells; MES-GSCs, mesenchymal glioma stem-like cells; DNA, deoxyribonucleic acid; ALDH1A3, aldehyde dehydrogenase subtype 1A3; ALDH1A1, aldehyde dehydrogenase subtype 1A1; ALDH1A2, aldehyde dehydrogenase subtype 1A2.

References

(1) Batash, R.; Asna, N.; Schaffer, P.; Francis, N.; Schaffer, M.; Glioblastoma Multiforme, Diagnosis and Treatment; Recent Literature Review. *Curr. Med. Chem*. **2017**, *24*, 3002-3009.

(2) Delgado-López, P. D.; Corrales-García, E. M. Survival in Glioblastoma: a Review on the Impact of Treatment Modalities. *Clin. Transl. Oncol*. **2016**, *18*, 1062-1071.

(3) Meacham CE, Morrison SJ. Tumour Heterogeneity and Cancer Cell Plasticity. *Nature*. **2013**, *501*, 328-337

(4) Tabassum DP, Polyak K. Tumorigenesis: it Takes a Village. *Nat. Rev. Cancer*. **2015**; *15*, 473-483.

(5) Pattabiraman DR, Weinberg RA. Tackling the Cancer Stem Cells – What Challenges Do They Pose? *Nat. Rev*. **2014**, *13*, 497-512.

(6) Singh, S. K.; Hawkins, C.; Clarke, I. D.; Squire, J. A.; Bayani, J.; Hide, T.; Henkelman, R. M.; Cusimano, M. D.; Dirks, P. B. Identification of Human Brain Tumour Initiating Cells. *Nature*. **2004**, *432*, 396-401.

(7) Ginestier, C.; Liu S.; Diebel, M. E.; Korkaya, H.; Luo, M.; Brown, M.; Wicinski, J.; Cabaud, O.; Charafe-Jauffret, E.; Birnbaum, D.; Guan, J. L.; Dontu, G.; Wicha, M. S. CXCR1 Blockade Selectively Targets Human Breast Cancer Stem Cells in Vitro and in Xenografts. *J. Clin. Invest*. **2010**, *120*, 485-497.

(8) Xiewan, C.; Rongxia, L.; Dezhi, L.; Jianguo, S. Induced Cancer Stem Cells Generated by Radiochemotherapy and their Therapeutic Implications. *Oncotarget*. **2017**, *8*, 17301-17312.

(9) Nunes, T.; Hamdan, D.; Leboeuf, C.; El Bouchtaoui, M.; Gapihan, G.; Nguyen, T. T.; Meles, S.; Angeli, E.; Ratajczak, P.; Lu, H.; Di Benedetto, M.; Bousquet, G.; Janin, A. Targeting Cancer Stem Cells to Overcome Chemoresistance. *Int. J. Mol. Sci*. **2018**, *19*, 4036-4060.

(10) Zhang, W.; Liu, Y.; Hu, H.; Huang, H.; Bao, Z.; Yang, P.; Wang, Y.; You, G.; Yan,W.; Jiang,T.; Wang, J. Zhang, W. ALDH1A3: a Marker of Mesenchymal Phenotype in Gliomas Associated with Cell Invasion. *PLoS ONE*. **2015**, *10*, e0142856.

(11) Mao, P.; Joshi, K.; Li, J.; Kim, S. H.; Li, P.; Santana-Santos, L.; Luthra, S.; Chandran, U. R.; Benos, P. V.; Smith, L.; Wang, M.; Hu, B.; Cheng, S. Y.; Sobol, R. W.; Nakano, I. Mesenchymal Glioma Stem Cells are Maintained by Activated Glycolytic Metabolism Involving Aldehyde Dehydrogenase 1A3. *Proc. Natl. Acad. Sci. USA*. **2013**, *110*, 8644-8649.

(12) Cheng, P.; Wang, J.; Waghmare, I.; Sartini, S.; Coviello, V.; Zhang, Z.; Kim, S. H.; Mohyeldin, A.; Pavlyukov, M. S.; Minata, M.; Valentim, C. L.; Chhipa, R. R.; Bhat, K. P.; Dasgupta, B.; La Motta, C.; Kango-Singh, M.; Nakano, I. FOXD1-ALDH1A3 Signaling is a Determinant for the Self-renewal and Tumorigenicity of Mesenchymal Glioma Stem Cells. *Cancer Res*. **2016**, *76*, 7219-7230.

(13) Sobreira, T. J. P.; Marlétaz, F.; Simões-Costa, M.; Schechtman, D.; Pereira, A. C.; Brunet, F.; Sweeney, S.; Pani, A.; Aronowicz, J.; Lowe, C. J.; Davidson, B.; Laudet, V.; Bronner, M.; Paulo de Oliveira, P. S. L.; Schubert, M.; Xavier-Neto, J. Structural Shifts of Aldehyde Dehydrogenase Enzymes were Instrumental for the Early Evolution of Retinoid-dependent Axial Patterning in Metazoans. *Proc. Natl. Acad. Sci. U. S. A.* **2011**, *108*, 226-231.

(14) Moretti, A.; Li, J.; Donini, S.; Sobol, R. W.; Rizzi, M.; Garavaglia, S. Crystal Structure of Human Aldehyde Dehydrogenase 1A3 Complexed with NAD^+ and Retinoic Acid. *Sci. Rep*. **2016**, *19*, 35710-35721.

(15) Verdonk, M. L.; Cole, J. C.; Hartshorn, M. J.; Murray, C. W.; Taylor, R. D. Improved Protein-ligand Docking using GOLD. *Proteins*. **2003**, *52*, 609-623.

(16) Morgan, C. A.; Hurley, T. D. Development of a High-throughput in Vitro Assay to Identify Selective Inhibitors for Human ALDH1A1. *Chem.-Biol. Interactions*. **2015**, *234*, 29-37.

(17) Chen, Y.; Zhu, J. Y.; Hong, K. H.; Mikles, D. C.; Georg, G. I.; Goldstein, A. S.; Amory, J. K.; Schönbrunn, E. Structural Basis of ALDH1A2 Inhibition by Irreversible and Reversible Small Molecule Inhibitors. *ACS Chem. Biol*. **2018**, *13*, 582-590.

(18) Gerencser, J.; Panka, G,; Nagy, T.; Egyed, O.; Dorman, G.; Uerge, L.; Darvas, F. Procedure for the Parallel Preparation of 3-Imidazo[1,2-*a*]pyridin-3-yl Propionic Acid Derivatives Involving Meldrum's acid. *J. Combi. Chem*. **2005**, *7*, 530-538.

(19) Bollenbach, M.; Salvat, E.; Daubeuf, F.; Wagner, P.; Yalcin, I.; Humo, M.; Letellier, B.; Becker, L. J.; Bihel, F.; Bourguignon, J.-J.; Villa, P.; Obrecht, A.; Frossard, N.; Barrot, M.; Schmitt, M. Phenylpyridine-2-ylguanidines and Rigid Mimetics as Novel Inhibitors of TNFα

Overproduction: Beneficial Action in Models of Neuropathic Pain and of Acute Lung Inflammation. *Eur. J. Med. Chem*. **2018**, *147*, 163-182.

(20) Michaelis, L.; Menten, M. L. Die Kinetik der Invertinwirkung. *Biochemische Zeitschrift*. **1913**, *49*, 333-369.

(21) SigmaPlot Extract Graphs and Data Analysis (StatSys v12.3).

(22) Kabsch W. XDS. *Acta Crystallogr. D Biol. Crystallogr*. **2010**, *66*, 125-32.

(23) Collaborative Computational Project, Number 4. The CCP4 suite: Programs for Protein Crystallography. *Acta Crystallogr. D Biol. Crystallogr*. **1994**, *50*, 760-763.

(24) McCoy, A. J.; Grosse-Kunstleve, R. W.; Adams, P. D.; Winn, M. D.; Storoni, L. C.; Read, R. J. Phaser Crystallographic Software. *J. Appl. Crystallogr*. **2007**, *40*, 658-674.

(25) Murshudov, G. N.; Vagin, A. A.; Dodson, E. J. Refinement of Macromolecular Structures by the Maximum-likelihood Method. *Acta Crystallogr*. **1997**, *D53*, 240-255.

(26) Afonine, P. V., Grosse-Kunstleve, R. W.; Echols, N.; Headd, J. J.; Moriarty, N. W.; Mustyakimov, M.; Terwilliger, T. C.; Urzhumtsev, A.; Zwart, P. H.; Adams, P. D. Towards Automated Crystallographic Structure Refinement with Phenix.refine. *Acta Crystallogr. D Biol. Crystallogr*. **2012**, *68*, 352-67.

(27) Emsley, P.; Lohkamp, B., Scott, W. G.; Cowtan, K. Features and Development of Coot. *Acta Crystallogr. D Biol. Crystallogr*. **2010**, *66*, 486-501.

(28) Brunger, A. T. Free R Value: a Novel Statistic Quantity for Assesing the Accuracy of Crystal Structures. *Nature*. **1992**, *355*, 472-475.

(29) Perrakis, A.; Harkiolaki, M.; Wilson, K. S.; Lamzin, V. S. ARP/wARP and Molecular Replacement. *Acta Crystallogr. D Biol. Crystallogr*. **2001**, *57*, 1445-1450.

(30) Schrödinger LLC (2010) The PyMOL Molecular Graphics System, version 1.3.

(31) Verdonk, M. L.; Cole, J. C.; Hartshorn, M. J.; Murray, C. W.; Taylor, R. D. Improved Protein-ligand Docking Using GOLD. *Proteins*. **2003**, *52*, 609-623.

(32) Jones, G.; Willett, P.; Glen, R. C.; Leach, A. R.; Taylor, R. Development and Validation of a Genetic Algorithm for Flexible Docking. *J. Mol. Biol*. **1997**, *267*, 727-748.

(33) Kim, S. H.; Ezhilarasan, R.; Phillips, E.; Gallego-Perez, D.; Sparks, A.; Taylor, D.; Ladner, K.; Furuta, T.; Sabit, H.; Chhipa, R.; Cho, J. H.; Mohyeldin, A.; Beck, S.; Kurozumi, K.; Kuroiwa, T.; Iwata, R.; Asai, A.; Kim, J.; Sulman, E. P.; Cheng, S. Y.; Lee, L. J.; Nakada, M.; Guttridge, D.; DasGupta, B.; Goidts, V.; Bhat, K. P.; Nakano, I. Serine/Threonine Kinase MLK4 Determines Mesenchymal Identity in Glioma Stem Cells in an NF-κB-dependent Manner. *Cancer Cell*. **2016**, *29*, 201-213.

Table of Content Graphic

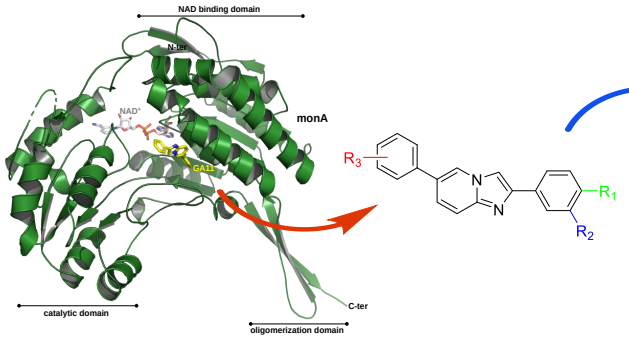

Anti-proliferative activity against GSC lines

	157	**267**	**374**
3b (IC_{50})	25.2 nM	63.4 nM	2.58 pM